WORCESTER POLYTECHNIC INSTITUTE

Preparation and Characterization of Composite PES/Nanoparticle Membranes

A Major Qualifying Project submitted to the faculty of Worcester Polytechnic Institute in partial fulfillment of the requirements for the Degree of Bachelor of Science in Environmental Engineering

Submitted by Patrick Sheppard

4/25/2013

Submitted to:

Project Advisor: Professor DiBiasio, Worcester Polytechnic Institute

Project Advisor: Professor Chi, Shanghai Jiao Tong University

Abstract

Membrane fouling remains an obstacle to widespread adoption of membrane technologies, and improving the hydrophilicity of a membrane's surface reduces membrane fouling. Therefore, there has been significant interest in improving membrane hydrophilicity. Many researchers have accomplished this by imbedding inorganic nanoparticles, often metal oxides, on polymeric membrane surfaces. These studies show that antifouling performance is significantly improved after the addition of inorganic nanoparticles. However, despite this multitude of studies that demonstrate the effectiveness of this technique, no study has critically analyzed which nanoparticle is most effective at reducing fouling. This study helps to fill this research gap. Four different nanoparticles TiO_2, SiO_2, ZnO, and ZrO_2, were dispersed in a polyethersulfone (PES) casting solution at 1 wt %, and composite membranes were then prepared from this casting solution via the phase inversion method. The resulting membranes' properties were characterized, and the results were compared. Of the four particles tested, SiO_2 displayed the best antifouling performance.

Contents

Table of Figures

Table of Tables

Introduction

According to the World Health Organization (2009), water scarcity is a growing issue that affects one in three people on every continent. Population growth, urbanization, increased standards of living, and the expansion of industrial activities are exacerbating this issue (Choi et al., 2002). Therefore, there is a growing need for better water resource management, which includes more effective water and wastewater treatment technologies. Of these technologies, membrane treatment is particularly promising. Zhou and Smith (2002) explain that membrane processes offer several advantages over conventional treatment processes: they are able to produce high quality effluent for a diverse range of inputs, do not require chemical addition under most circumstances, reduce the amount of solids disposal, occupy a small amount of space, are easy to control, and reduce operation and maintenance costs.

However, membrane fouling remains an obstacle to widespread adoption of membrane technologies (Meng et al., 2009). Huang et al. (2012) explain that membrane fouling is caused by the deposition of pollutants on the membrane surface or from adsorption of pollutants into membrane pores. It leads to reduced flux and therefore increased energy usage over time. It also often creates the need for chemical cleaning, which further increases cost and maintenance requirements (Huang et al., 2012).

Currently, organic polymers are the most commonly used materials for commercial membranes (Zhou and Smith, 2002). However, organic polymers have a hydrophobic surface which, as observed in many studies, makes them particularly susceptible to membrane fouling (Su et al., 2011; Yu et al., 2005; Choi et al., 2002). Fouling is more severe in hydrophobic membranes because of hydrophobic interactions between solutes, microbial cells, and membrane material (Choi et al., 2002).

As a result, there has been significant interest recently in discovering ways to improve the hydrophilicity of organic polymer membranes (Shen et al., 2011). Wu et al. (2008) explain that several methods have been employed to modify membrane surfaces to make them more hydrophilic, including the application of ultraviolet radiation, blending with hydrophilic materials, graft polymerization, and plasma grafting. Of these methods, blending with hydrophilic materials, particularly inorganic nanoparticles, has attracted the most attention because it requires mild synthesis conditions during membrane preparation (Genne, Kuypers and Leysen, 1996).

Li et al. (2008) write that there are three methods commonly used to blend inorganic materials with polymer membranes: (1) disperse nanoparticles in the casting solution directly and prepare the composite membranes via phase inversion; (2) add prepared sol containing nanoparticles in the casting solution and prepare the composite membranes via phase inversion; and (3), dip the prepared membrane in an aqueous suspension containing nanoparticles and prepare the composite membranes via self-assembly. Several studies have applied these methods to blend different nanoparticles with organic polymer membranes. The nanoparticles used include TiO_2 (Li et al., 2009; Wu et al., 2008) SiO_2 (Huang et al., 2012; Shen et al., 2011), ZrO_2 (Maximous et al.,

2010; Bottino, Capannelli and Comite, 2002; Genne, Kuyperes and Leysen, 1996), and ZnO (Shen et al., 2012).

Of these nanoparticles, TiO_2 has been studied the most thoroughly due to its stability, availability, (Wu et al., 2008) high hydrophilicity, and photocatalytic potential (Li et al., 2009). Jing-Feng Li et al. (2009) dispersed varying concentrations of TiO_2 nanoparticles (0-5 wt %) in polyethersulfone (PES) casting solutions and prepared composite membranes via phase inversion. They found that the composite membranes had enhanced thermal stability, hydrophilicity, and permeation performance. They recommended an optimal loading rate of 1-2 wt % TiO_2. Wu et al. (2008) also prepared TiO_2/PES composite membranes via nanoparticle dispersion and phase inversion. They confirmed Jing-Feng Li et al.'s findings that the addition of TiO_2 enhanced the hydrophilicity, thermal stability, and mechanical strength of the membrane. However, they recommended an optimal TiO_2 loading rate of 0.5 wt % rather than 1-2 wt %. Jian-Hua Li et al. (2008) modified poly (styrene-alt-maleic anhydride)/poly(vinylidene fluoride) (SMA/PVDF) to contain TiO_2 nanoparticles via the self-assembly method. They also confirmed that the modified membranes had enhanced hydrophilicity and superior permeability.

SiO_2, though not as widely studied as TiO_2, has also been analyzed. Shen et al. (2011) prepared PES/SiO_2 composite membranes (0-5 wt % SiO_2) by the phase inversion method. They found that pure and raw water flux increased, hydrophilicity was enhanced, and anti-fouling ability increased with the addition of SiO_2. Huang et al. (2012) prepared mesoporous silica (MS) modified PES membranes via phase inversion. They found that the MS improved membrane hydrophilicity, porosity, anti-fouling ability, and thermal stability. They recommend an optimal MS loading rate of 2 wt %.

A third nanoparticle that has been studied for membrane modification is ZrO_2. Maximous et al. (2010) prepared PES/ZrO_2 composite membranes (0, 0.01, 0.03, 0.05, 0.07, and 0.1 PES/ZrO_2 weight ratios) via phase inversion and used these membranes for activated sludge filtration to study their fouling characteristics. They found that the addition of ZrO_2 particles improved mechanical strength and anti-fouling ability. They recommend an optimal ZrO_2 loading rate of 0.05 ZrO_2/PES. Two older studies (Bottino, Capannelli, and Comite, 2002; Genne, Kuypers and Leysen, 1996) also prepared ZrO_2 composite membranes. Though their analyses were not as thorough as those conducted by Maximous et al., both confirmed that permeability increased with the addition of ZrO_2.

Though less studied than the three other aforementioned particles, ZnO's effect on membrane performance has also been analyzed. Shen et al. (2012) prepared PES/ZnO composite membrane via phase inversion. They found that the addition of ZnO imporves hydrophilicity, thermal decomposition temperature, water flux, and porosity.

All these studies demonstrate the validity of the principle that the addition of nanoparticles can enhance membrane anti-fouling performance as well as many other membrane characteristics. However, despite this multitude of studies that demonstrate this principle, no study, to our

knowledge, has critically analyzed which nanoparticle is most effective at improving membrane performance. We hope this study helps to fill this research gap.

We studied the effect that the addition of four different nanoparticles, TiO_2, SiO_2, ZrO_2, and ZnO, will have on PES membranes. The nanoparticles were dispersed in a PES casting solution at 1 wt %. Composite membranes were then prepared from this casting solution via the phase inversion method. The resulting membranes' properties were characterized, and the results were compared.

Background

An abundant supply of clean, fresh water is important for human wellbeing. It is essential for numerous human activities, such as irrigated agriculture, which supplies much of the world's food; for many industrial processes, which help to fuel economic development; for human consumption and leisure, which help to keep us healthy and happy; and for energy production, which allows industrial societies to thrive (Pereira, Cordery, and Iacovides, 2009).

However, in many areas of the globe, an abundant supply of clean, fresh water does not exist – water scarcity now affects one in three people on every continent (World Health Organization). By 2025, an estimated 1.8 billion people will live in areas that are water scare (<1000 m^3 of water per capita per year), and two-thirds of the world's population will live in areas that are water stressed (<1700 m^3 of water per capita per year) (National Geographic). Figure 1 illustrates the areas of the globe most affected by water scarcity.

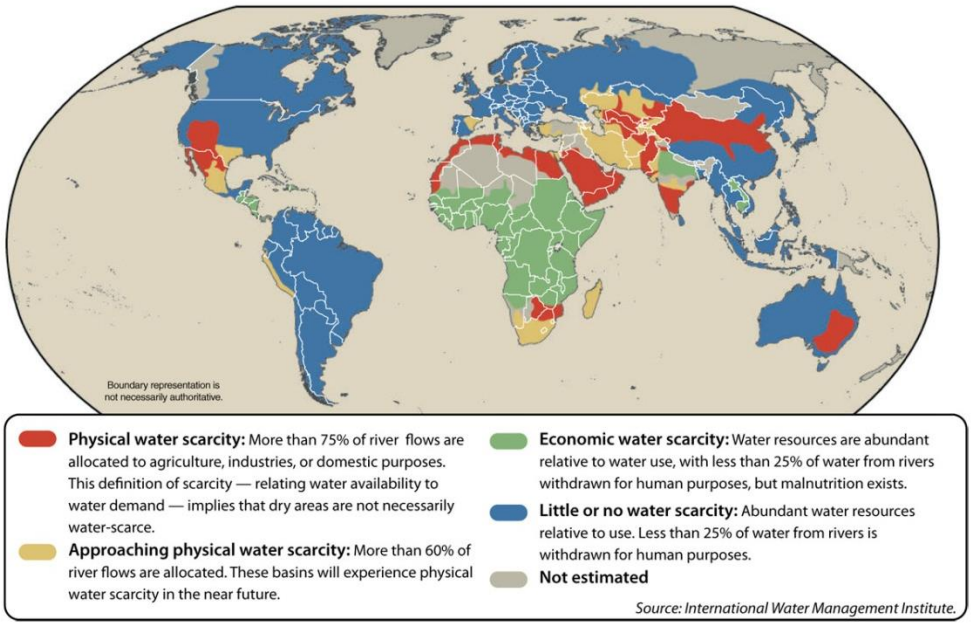

Figure 1: Projected global water scarcity by 2025

Not only is lack of water a growing issue, however, but poor water-quality is as well. Scientific knowledge has increased about the consequences of poor water quality on public and environmental health, and this increased awareness has led to increased regulation in many nations. Zhou and Smith (2002) explain that we (1) better understand the impacts of disinfection byproducts from conventional water-treatment methods, (2) have witnessed disease outbreaks caused by water contaminated with *Giardia* cysts and *Cryptosporidium* ocysts, and (3) have seen how nutrients, like nitrogen and phosphorous, as well as synthetic organic compounds, impact public health and the environment. These observations have led to further regulation. For example, The United States Environmental Protection Agency has proposed legislation such as

the Interim Enhanced Surface Water Treatment Rule and the Disinfection-Disinfection By-Product Rule (Zhou and Smith, 2002).

As a result of both this lack of water and of the increased scientific knowledge about the importance of water quality, the scientific community recognizes the need for a more abundant, high-quality water supply. Unfortunately, though, there are key challenges that make meeting this need difficult, including rapid population growth, industrialization, increased global living standards, and climate change. These challenges are discussed below.

Challenges to Meeting Global Water Demand

According to the Population Institute (2010), the world's population is increasing at a rate of 80 million people per year. This corresponds to an increase in fresh water demand of roughly 64 billion m^3 annually. By 2050, the population is expected to expand to 9 billion people, and much of this expansion will occur in developing countries, many of which are already experiencing water stress or water scarcity (Population Institute, 2010).

In addition to population growth, water use per capita is increasing as well, according to the World Water Organization (2010). This is the result of increasing standards of living. In the United States, a developed nation, residents use 100 to 176 gallons of water per day. Conversely, in Africa, the average family uses 5 gallons of water per day. As more countries, such as China, India, and Brazil, industrialize, water use per capita moves further from levels observed in Africa and nearer to levels observed in the United States. As a result of this trend, since 1950, the world population has doubled, but water use has tripled (World Water Organization, 2010).

Global warming is also expected to further exacerbate water scarcity in the future. According to Mcintyre (2012), temperature increases raise the amount of water in the atmosphere, which leads to heavier rainfall when the air cools. However, though this increases the amount of freshwater resources, it also increases the rate that these resources flow into the ocean. Also, the impact of global warming on water availability will be varied. In many areas that are already dry, rainfall is expected to decrease further and evaporation rates are expected to increase, threatening approximately 1 billion people who live in these already-dry locations (Mcintyre, 2012). Also, a report from the United Nations Food and Agriculture Organization (FAO, 2011) reports that glaciers, which support 40% of the world's agricultural irrigation, will recede and reduce the amount of surface water available for many farmers.

Due to these challenges, there is a growing need for better water resource management, which includes more effective water and wastewater treatment technologies. Three technologies – advanced oxidation processes (AOPs), UV irradiation, and membrane filtration – have been developed to meet these needs (Zhou and Smith, 2002). These three technologies are discussed briefly below.

Alternative Technologies

Advanced Oxidation Processes (AOPs)

Advanced oxidation processes, broadly, refer to a set of chemical reactions used to treat water and wastewater through the use of hydroxyl radicals (-OH). Poyatos and others (2010) write that these radicals are reactive, attack most organic molecules, and are not highly selective. They efficiently fragment and convert pollutants into small inorganic molecules, the authors continue. The generation of –OH radicals is accomplished by combining "ozone (O_3), hydrogen peroxide (H_2O_2), titanium dioxide (TiO_2), heterogeneous photocatalysis, UV radiation, ultrasound, and (or) high electron beam irradiation" (Zhou and Smith, 2002, p. 254). Figure 2 illustrates an AOP that uses ozone and hydrogen peroxide. The applications of AOPs, though, are diverse, and many are shown in Table 1.

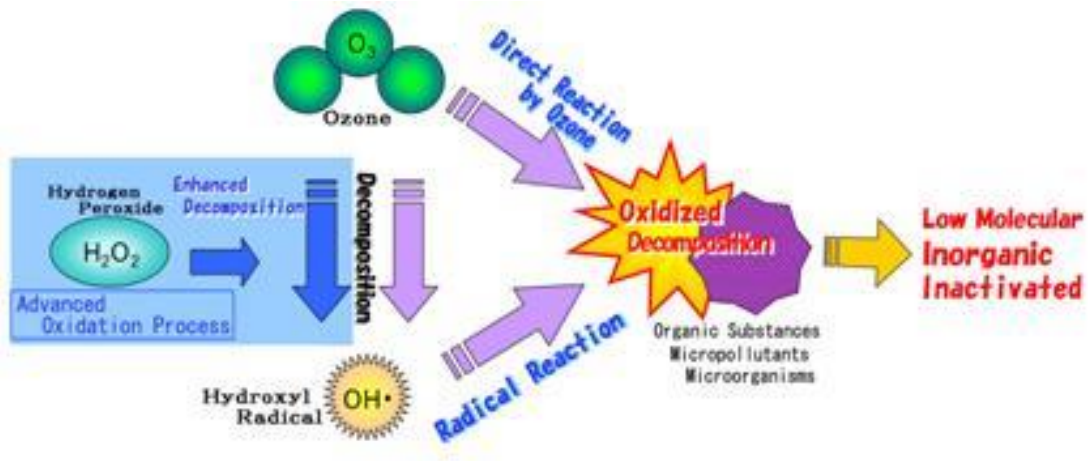

Figure 2: An example of an advanced oxidation process with Hydrogen Peroxide (Sewerage Business Management Centre)

Table 1: Summarizes some of the many applications of AOPs. This table was taken from Zhou and Smith (2002).

Processes	Applications	Resulting effects	References
O_3	Coagulation aid	Change in primary coagulant demand and floc stability; increase in Al and Fe residual in finished water	Grasso and Weber 1988
	Fe and Mn removal	Increase with ratio of O_3 to DOC; Fe^{2+} oxidation followed by Mn^{2+}; MnO_4^- ions may be formed with excessive O_3	Paillard et al. 1989
	Colour removal	70% colour reduction for pulp mill effluents in practice	Zhou and Smith 1997
	Taste and odour control	Effective reduction in taste and odour	Ferguson et al. 1990
	Algae removal	Enhancement of filtration for algae removal	Bernhardt and Lusse 1989
	SOC oxidation	Atrazine oxidation is a first-order reaction rate which is affected by pH, temperature, alkalinity, and NOM	Adams and Randtke 1992
	Disinfection	Increase with ozone residual; general effectiveness follows bacteria > virus > *Giardia* > *Cryptosporidium*	Foster et al. 1980; Gyürék et al. 1999
	DBP control	THMFP reduction with the ratio of O_3 to DOC	Reckhow and Singer 1984
	Bromate formation	Bromate formation via both molecular and radical mechanisms	von Gunten and Hoigne 1994
	AOC formation	Produce various aldehydes; increase BDOC and AOC	Paode et al. 1997
O_3–H_2O_2	SOC oxidation	Decrease 447 μg/L TCE and 163 μg/L PCE to below 5 μg/L in groundwater	Karimi et al. 1997
	Taste and odour reduction, DBP control, and disinfection	90% removal of MIB and geosmin at an ozone dose of 2 mg/L for O_3–H_2O_2 compared with 4 mg/L for O_3 alone; low DBP formation, and comparable inactivation	Ferguson et al. 1990
O_3, O_3–UV	Micropollutant destruction	TCE, NOM precursors, PCBs, trihalomethanes, chloroform, and bromodichloromethane were effectively oxidized	Peyton et al. 1982*a*, 1982*b*
H_2O_2–UV photolysis	SOC oxidation	99% removal of atrizane from both types of oxidation; the oxidation rate was faster with H_2O_2–UV	Beltran et al. 1993
UV–TiO_2, etc.	Hazardous compounds oxidation	Effective mineralization of TCE, toluence, MEK, and 2,4-DCP, as evidenced by substantial TOC reduction	Suri et al. 1993

Zhou and Smith (2002) specify four reasons AOPs are attractive processes.

1. They are effective at removing resistant organic compounds
2. They are capable of "complete mineralization of organic contaminant into carbon dioxide"
3. They are less susceptible to toxic chemicals
4. They produce fewer harmful by-products

However, despite these benefits, AOPs can also reduce the concentration of disinfectants in water, and thus are not advantageous during microbial disinfection. Also, they still remain costly.

UV Radiation

According to the United States EPA (1999), ultraviolet (UV) radiation does not inactivate microorganisms through a chemical reaction. Instead, it applies UV light, generally at wavelengths between 250 and 270 nm, to kill microorganisms. The UV radiation interacts with the nucleic acids of the microorganisms, therefore disabling their DNA and leaving them unable to reproduce and perform other vital cell functions. Figure 3 illustrates the impact of UV radiation on genetic material (U.S. EPA, 1999)

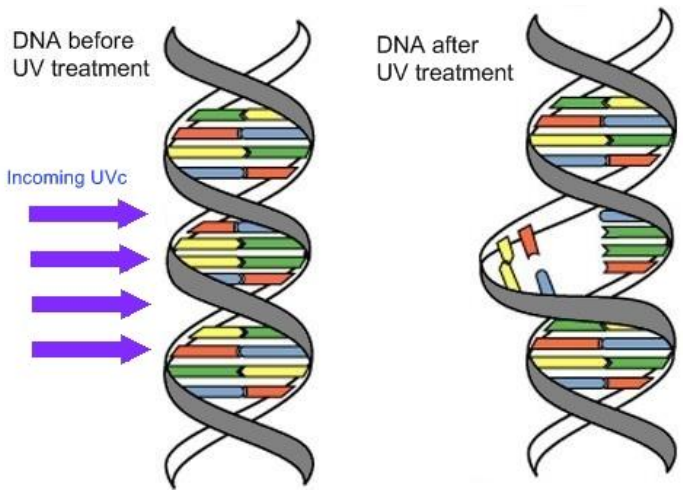

Figure 3: Impact of UV radiation on DNA. Demonstrates how UV radiation inactivates pathogens (DaRo UV)

According to the EPA (1999), UV radiation holds numerous advantages when compared to conventional treatment methods. It is effective at eliminating most viruses, spores, and cysts; it eliminates the need for chemical handling; there are no harmful residual effects post-treatment; it is user-friendly; and it requires very little space and also very little contact time (20 to 30 seconds) when compared to other disinfectants.

However, despite these advantages, the EPA (1999) also does recognize that there are disadvantages. It does not inactivate all pathogens; organisms can sometimes repair the damage UV radiation does to them; a maintenance program is necessary to control fouling in tubes; turbidity can render it ineffective; and it is not quite as cost-effective as chlorination.

Membrane Filtration

Membranes are semi-permeable barriers that separate materials based on their physical and/or chemical properties. Figure 4 illustrates a membrane process. In this process, a solution is passed over the membrane. Some of this solution, the permeate, travels through the membrane. Other parts of this solution, the retentate, do not. The passage of materials through a membrane generally requires a driving force, normally pressure (Davis and Masten, 2009).

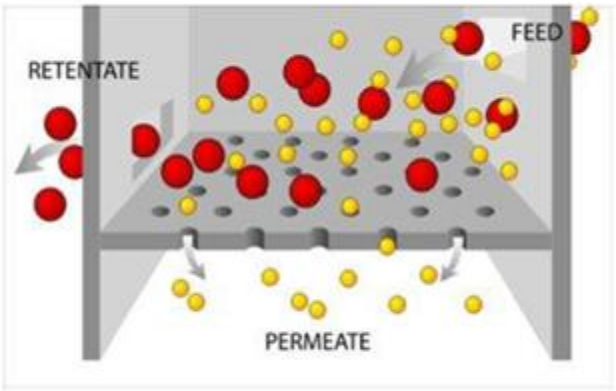

Figure 4: Illustration of a membrane process (Saddatt, 2011)

Zhou and Smith (2002) explain that membrane processes offer several advantages over conventional treatment processes: they are able to produce high quality effluent for a diverse range of inputs, do not require chemical addition under most circumstances, reduce the amount of solids disposal, occupy a small amount of space, are easy to control, and reduce operation and maintenance costs.

In addition, membranes are effective at treating small particles, like *Cryptosporidium* ocysts and *Giardia* cysts, that conventional methods generally miss. For these reasons, we studied membrane processes in this experiment. Therefore, more details about membrane processes, their advantages, and their disadvantages are discussed in the following section.

Membrane Processes: An Overview

Membrane Classification

According to Zhou and Smith (2002), membranes can be classified based on a number of different characteristics, such as the "mechanisms of rejection, the driving forces employed, the chemical structure and composition of the membranes, and the geometry of construction" (p. 248) However, the most important characteristic used to categorize membranes is maximum permeate particle size. Based on this characteristic, there are four primary categories of membrane processes: microfiltration (MF), ultrafiltration (UF), nanofiltration (NF), and reverse osmosis (RO) (Davis and Masten, 2009). Figure 5 summarizes the maximum permeate particle sizes of each of these four processes and also shows the sizes of some common pollutants.

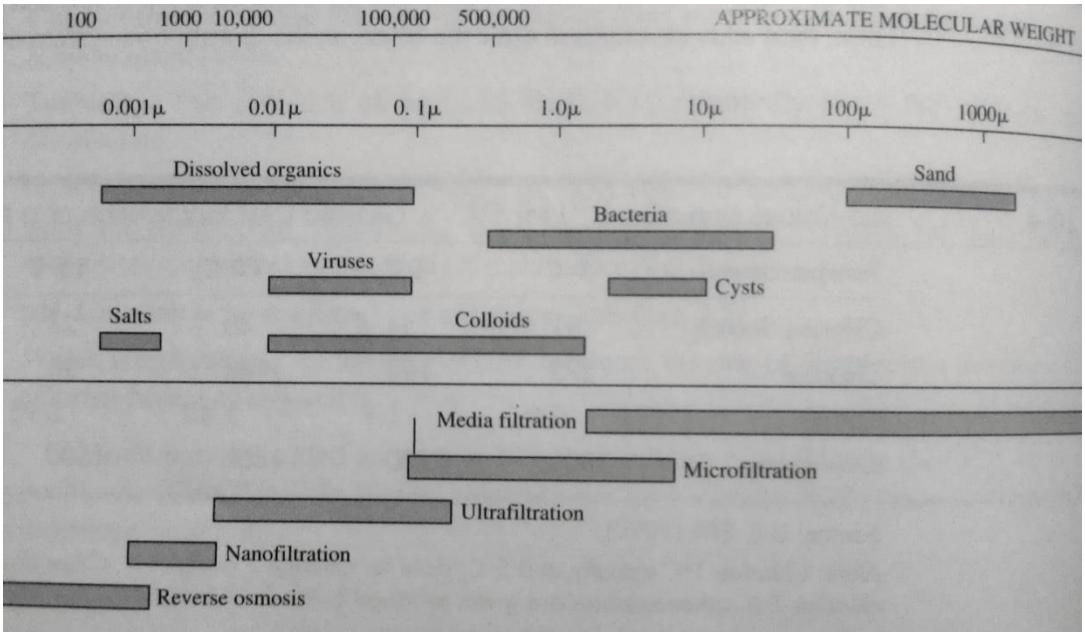

Figure 5: Illustration of the four major classifications of membranes based on permeate particle size, MF, UF, NF, and RO, as well as some of the sizes of many common pollutants (Davis and Masten, 2009).

As shown in Figure 5, MF membranes have the largest pore diameters – they are used to remove particles greater than 50 nm in size (Davis and Masten, 2009). As a result, they are capable of a relatively high flux, even when there is only a small pressure differential across the membrane (Zhou and Smith, 2002). MF membranes are able to achieve a several log reduction in bacteria, but only a 2-3 log reduction in viruses (Davis and Masten, 2009).

RO membranes, conversely, have very small pore sizes. They can be used for the removal of salts, ionic substances as small as 1-15 Å in diameter, and low molecular-weight dissolved organic chemicals. Unlike MF, they require high operating pressures that exceed the osmotic pressure of the water being treated (Davis and Masten, 2009).

Both UF and NF fall somewhere between MF and RO in terms of permeate particle size and required transmembrane pressure. Both are effective at removing natural organic matter (NOM) and trace synthetic organic compounds (SOCs) while maintaining a reasonable permeate flux (Zhou and Smith, 2002). The separation sizes and typical operating pressures of these membranes are summarized in Table 2.

Table 2: Summary of membrane classifications based on permeate particle size.

Membrane	Separation Size (μm)	Main Mechanisms	Typical Transmembrane pressure (MPa)	Permeate Flux
RO	<0.001	Diffusion + Exclusion	5-8	Low
NF	0.001-0.008	Diffusion + Exclusion	0.5-1.5	Medium
UF	0.003-0.1	Sieving	0.05-0.5	High
MF	>0.05	Sieving	0.03-0.3	High

Membrane Fouling

Though diverse in structure and performance, there are still drawbacks that apply to nearly all membrane processes. The biggest of these drawbacks is membrane fouling, which is primarily responsible for preventing the widespread adoption of membrane technologies (Davis and Masten, 2009). Membrane fouling is caused by the deposition of pollutants on the membrane surface or from adsorption of pollutants into membrane pores (Huang et al., 2012). It leads to reduced flux and therefore increased energy usage over time. It also often creates the need for chemical cleaning, which further increases cost and maintenance requirements (Huang et al., 2012). This section provides further background on membrane fouling.

Description of Membrane Fouling

Marshall, Munro and Tragardh (1993) write that flux loss due to fouling occurs in three phases. These three phases are shown in Figure 6. In the first phase, which lasts approximately one minute, flux loss is primarily caused by concentration polarization. Figure 7 illustrates concentration polarization. Concentration polarization occurs because the solute that is rejected by the membrane builds up at the membrane surface. The concentration of this solute, then, is higher at the membrane surface (C_m) than it is in the bulk solution (C_b). If C_m grows large enough, a gel layer with solute concentration C_g forms. This gel layer adds additional resistance (R_g) that, ultimately, reduces the flux (McCabe, Smith and Harriott, 1956).

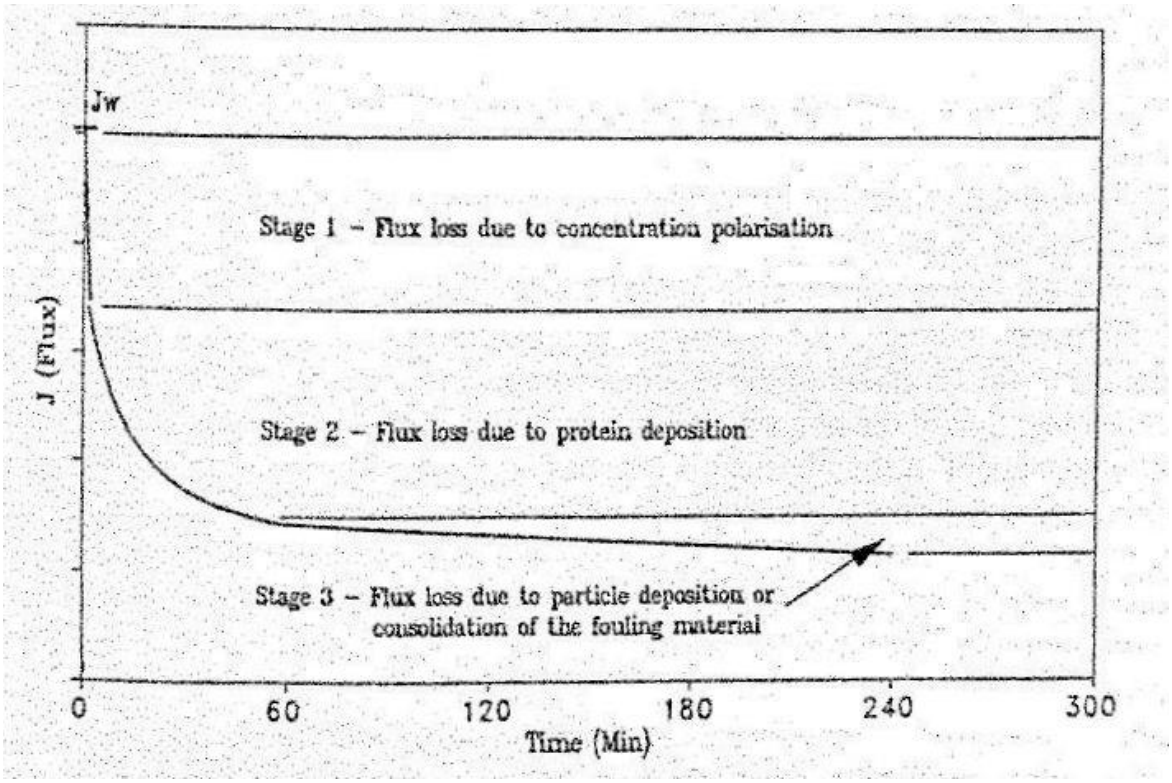

Figure 6: The three phases of fouling. In the first phase, which lasts roughly one minute, flux loss is primarily caused by concentration polarization. In the second phase, which lasts between one and three hours, the flux declines at a moderate rate due to protein deposition on the membrane surface. And in the final phase, which continues indefinitely, the flux declines slowly due to further protein deposition.

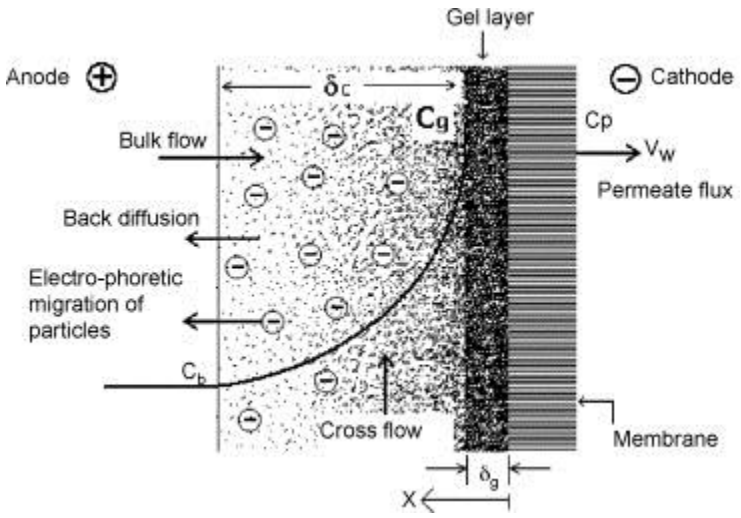

Figure 7: Illustration of concentration polarization, which leads to the first phase of flux loss during membrane filtration.

Concentration polarization is dictated by the hydrodynamic conditions of the membrane system (Marshall et al., 1993). It can be controlled by a "cross-flow membrane module by means of

construction," velocity adjustment, pulsation, ultrasound, or electric field generation (Koltuniewicz and Noworyta) and is always reversible.

In the second phase of flux decline, the flux decreases moderately and is a result of protein deposition on the membrane surface. It is likely that proteins initially adsorb onto the membrane surface as a monolayer until a complete surface layer forms, resulting in reduced membrane flux.

The third phase of flux decline occurs when there is further protein deposition onto this monolayer.

Although Goosen et al. (2005) explain that a number of different substances can cause fouling, including bacteria, humic acids, and inorganics, this study focuses on fouling caused by proteins because proteins were the only pollutants that this study tested experimentally. It is generally accepted that protein adsorption, however, plays an important role in membrane fouling (Marshall et al., 1993).

Protein adsorption occurs for two primary reasons. First, according to the Derjaguin, Landau, Verwey, and Overbeek (DLVO) Theory, biomolecules and colloidal particle typically carry a negative charge. This charge is reduced by the adsorption of counter ions, and an electrical double layer forms, as shown in Figure 8.

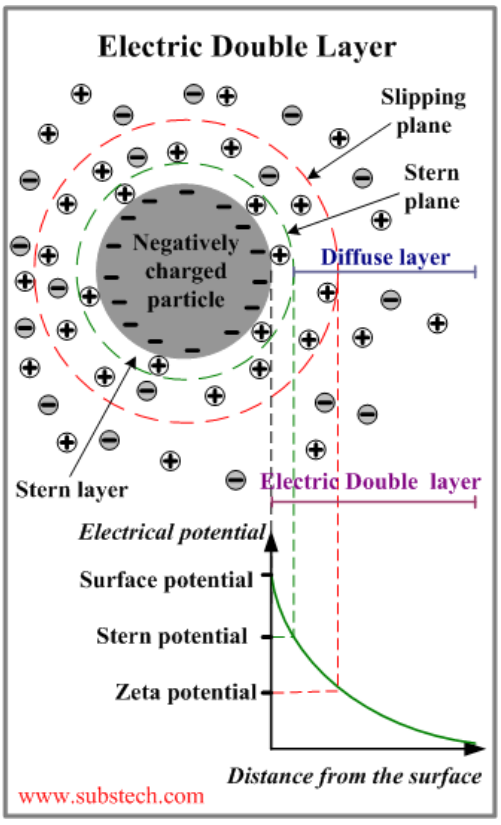

Figure 8: Illustration of the electrical double layer that forms around charged particles (http://www.substech.com/dokuwiki/lib/exe/fetch.php?w=&h=&cache=cache&media=electric_double_layer.png)

This double layer results in electrostatic repulsion forces. However, Van der Waals forces lead to attraction. The energy of interaction is the sum of both these attractive and repulsive forces and is a function of the distance between a particle and the membrane surface. If the molecule and the membrane surface have opposite charges, it is likely that there will be electrostatic attraction. Figure 9 summarizes the DLVO Theory.

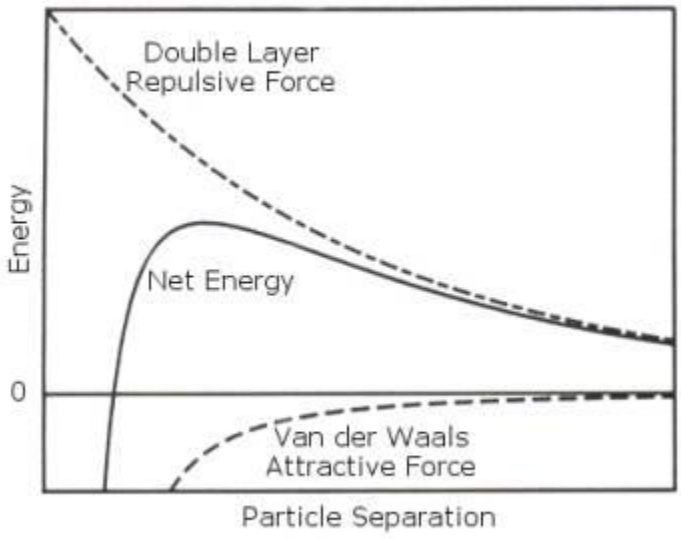

Figure 9: Graphical representation of the DLVO Theory (http://www.malvern.com/labeng/industry/colloids/dlvo_theory_1.jpg)

And second, hydrophobic interactions can lead to protein adsorption as well. Water molecules form hydrogen bonds with themselves and with hydrophilic surfaces. The intrusion of hydrophobic surfaces "disrupts this ordered structure and is thus energetically unfavorable (70)." Therefore, entropy is increased if hydrophobic contact is minimized, and this results in strong hydrophobic interactions. Figure 10 illustrates this phenomenon. Because of hydrophobic interactions, if both a pollutant and the membrane surface are hydrophobic, they are more likely to interact, and fouling is more likely to result.

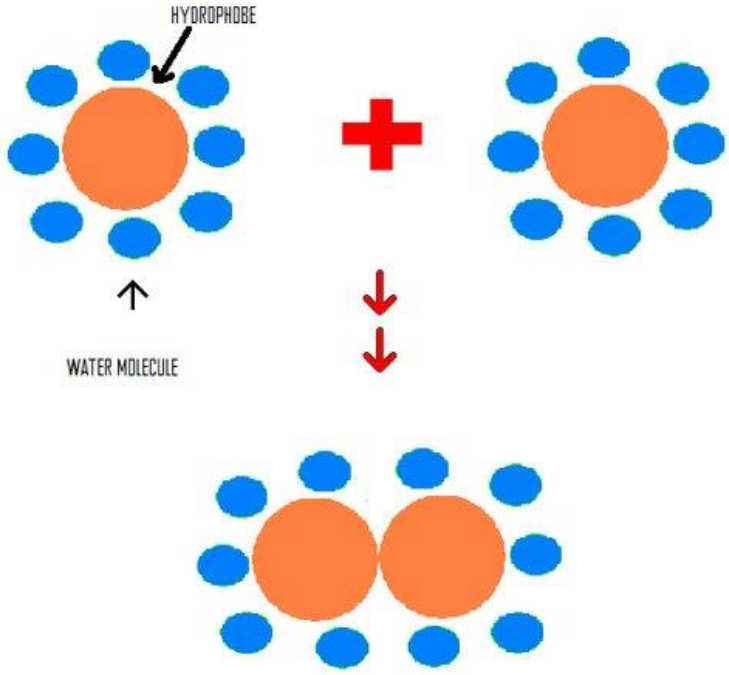

Figure 10: Illustration of hydrophobic interactions among components in water. These hydrophobic interactions increase contact between hydrophobic membrane surfaces and hydrophobic foulants in wastewater which leads to increased fouling. (http://chemwiki.ucdavis.edu/Physical_Chemistry/Physical_Properties_of_Matter/Intermolecular_Forces/Hydrophobic_interactions)

In addition to adsorption on the protein surface, Marshall et al. (1993) explains that protein fouling can occur inside the membrane's pores. Within membranes pores, fouling is small when compared with membrane surface fouling. It is greatest during MF, and the largest amount of fouling appears to occur in larger pores.

Types of Membrane Fouling

There are three different types of membrane fouling reported in the literature: reversible fouling, irreversible fouling, and irrecoverable fouling. According to Radjenovic et al. (2008), reversible fouling is fouling that can be removed by physical membrane cleaning. It is caused by foulants that are poorly adsorbed onto the membrane surface. Irreversible fouling is fouling that cannot be removed by physical cleaning but can be removed by chemical cleaning. And last, irrecoverable fouling is fouling that cannot be removed by any cleaning methods. Reversible fouling is the type of fouling that is most conducive to lower membrane operation costs (Radjenovic et al. 2008).

It is also important to note that fouling is a complex and poorly understood process that varies largely based on membrane properties and membrane operating parameters. Marshall, Munro and Tragardh (1993) examined some of these factors that affect membrane fouling, and the results of this analysis are presented below. Unless otherwise noted, the information presented below comes from their paper.

Parameters that Impact Membrane Fouling

Feed Concentration

Increasing the feed concentration, in general, decreases the permeate flux. It also increases reversible surface fouling, although it appears to have little impact on irreversible surface fouling. However, it does increase the rate of membrane fouling when internal pore fouling dominates.

pH and Ionic Strength

The effect of pH and ionic strength on fouling is poorly understood, likely because it varies so much depending on the protein and the membrane being studied. However, it does impact fouling performance, though these impacts are variable depending on the system being analyzed. Nevertheless, three general explanations have been provided for the effect of pH and ionic strength on fouling. First, changes in protein "conformation and stability affect the tendency of the protein to deposit on the membrane" (p. 83) Second, changes in the charge difference between the protein and the membrane surface affect fouling. And third, changes in the protein's effective size "alter the porosity of the dynamic membrane" (p. 83).

Pre-filtration and the removal of aggregates

Pre-filtration and clarification of the feed material have both been shown to increase protein flux during membrane filtration. Both these processes remove larger protein aggregates from the bulk solution, and therefore these larger molecules cannot block membrane pores. This results in reduced fouling.

Component Interactions

Component interactions in the bulk solution can impact membrane performance in a couple ways. First, the presence of a larger component can increase the retention rate of smaller components. This may be because, if the larger molecules are sufficiently retained by the membrane, they could form a secondary membrane which reduces the passage of smaller molecules through the primary membrane. Also, larger molecules pass more slowly, due to friction, through membrane pores, which could further reduce the rate of passage of smaller molecules. And last, in certain cases, specific component interactions within the feed can affect retention rates.

Hydrophobicity

Reihanian, Robertson and Michaels (1983) found that filtration of a BSA solution through three hydrophobic membranes (XM200, XM50, and PM30) led to reduced flux over time. This is likely due to BSA adsorption on the membrane surface. However, when BSA solution was filtered through highly hydrophilic cellulosic YM30 and poly-ion complex UM10 membranes, there was no flux decline, indicating that were also was no BSA adsorption. This suggests that hydrophilic membranes foul less easily than hydrophobic ones, a finding that has been widely reproduced. Sheldon et al. suggest that one of the reasons for increased fouling on hydrophobic membranes is that hydrophobic membrane surfaces help to denature proteins. They found that "the tertiary protein structure of the globular protein [BSA] had, in some way, been disrupted and distorted by

interaction between BSA and polysulphone." Normally, the outer layer of BSA is hydrophilic, but, in this experiment, the BSA molecules adsorbed on the membrane surface had their hydrophobic sites exposed.

Charge

The charge of the membrane surface is dependent on a number of factors including the PH and ionic strength of the feed solution and the membrane material. Generally speaking, higher permeate fluxes are observed if the charge of the membrane is similar to that of the protein being filtered.

Surface roughness

An increase in surface roughness increases the likelihood of protein adsorption. However, it also affects "the nature of the dynamic membrane" (p. 88). A rough membrane surface can reduce the "completeness" of the dynamic membrane, which can in turn impact fouling.

Porosity and pore size distribution

Porosity and pore size distribution are important parameters in membrane performance. They have a large impact on membrane selectivity; membranes with a wide pore size distribution will be less selective than membranes with a low pore size distribution, assuming the average pore sizes are the same.

Also, porosity and pore size distribution impact fouling. In general, membrane fouling is most prevalent in membranes with low porosity and high heterogeneity. Greater heterogeneity leads to a greater velocity normal to the membrane surface, which increases the rate of protein deposition, which in turn leads to greater fouling.

Fouling can also impact the pore size distribution on a membrane surface. Studies have shown that when fouling occurs, porosity and pore size distribution both decrease. Small pores become blocked, and large pores decrease in size. This leads to a reduction in the number of small and large pores and an increase in the number of medium sized pores.

Pore size

Pore size affects membrane performance in several ways. Many researchers have observed that increased pore size, and thus decreased intrinsic membrane resistance, leads to increased membrane fouling and, in some cases, lower permeate flux. Because of this, there is an optimal pore size for particular membrane systems. Below this optimal pore size, membrane resistance dominates and restricts permeate flow. Above this optimal pore size, fouling dominates and restricts permeate flow. This optimal pore size is dependent on velocity.

Also, pore size is not necessarily the most important factor; rather, but the protein to pore size ratio may be more important.

Transmembrane pressure

Increasing transmembrane pressure (TMP) increases permeate flux but also increases protein fouling. However, there is an optimal TMP, and after this point, further increasing the TMP will not lead to an increase in permeate flux. This optimal TMP decreases as pore size increases.

Higher TMP, studies found, also led to lower flux recovery after flushing, which suggests that more fouling occurred when compared to lower TMP.

Cross-flow velocity and turbulence promoters

Generally, increasing cross-flow velocity results in an increase in permeate flux. Membrane resistance decreases, which suggests that fouling and concentration polarization decrease as well. Increased flux recovery is associated with higher cross flow velocity as well, which, again, suggests less membrane fouling occurs.

Backflushing

The results of backflusing in UF and MF are varied. Some studies show that it is effective, while others observe little difference. If accumulation of particles takes place on the membrane surface, backflushing will likely be effective. However, if accumulation of particles takes place in membrane pores or if particles are tightly adsorbed onto the membrane surface, backflushing will likely not be very effective.

Temperature

Generally, increasing the temperature lowers the viscosity of the permeate and increases permeate flux. In addition, it increases diffusivity, which helps to disperse the polarized layer in membrane filtration.

Strategies to Address Membrane Fouling

Taking to consideration all of these factors that impact membrane fouling performance, several strategies have been developed to help reduce membrane fouling, including microfiltration, coagulation and flocculation, and membrane surface-modification. This study focuses on membrane surface modification.

Membrane Surface Modification

Currently, organic polymers are the most commonly used materials for commercial membranes. However, organic polymers have a hydrophobic surface which, as observed in many studies, makes them particularly susceptible to membrane fouling (Su et al., 2011; Yu et al., 2005; Choi et al., 2002). Fouling is more severe in hydrophobic membranes because of hydrophobic interactions between solutes, microbial cells, and membrane material (Choi et al., 2002).

As a result, there has been significant interest recently in discovering ways to improve the hydrophilicity of organic polymer membranes (Shen et al., 2011). Wu et al. (2008) explain that several methods have been employed to modify membrane surfaces to make them more hydrophilic, including the application of ultraviolet radiation, blending with hydrophilic materials, graft polymerization, and plasma grafting. Of these methods, blending with hydrophilic

materials, particularly inorganic nanoparticles, has attracted the most attention because it requires mild synthesis conditions during membrane preparation (Genne, Kuypers and Leysen, 1996).

Li et al. (2008) write that there are three methods commonly used to blend inorganic materials with polymer membranes: (1) disperse nanoparticles in the casting solution directly and prepare the composite membranes via phase inversion; (2) add prepared sol containing nanoparticles in the casting solution and prepare the composite membranes via phase inversion; and (3), dip the prepared membrane in an aqueous suspension containing nanoparticles and prepare the composite membranes via self-assembly (Li et al., 2009). Several studies have applied these methods to blend different nanoparticles with organic polymer membranes. The nanoparticles used include TiO_2 (Li et al., 2009; Wu et al., 2008) SiO_2 (Huang et al., 2012; Shen et al., 2011), ZrO_2 (Maximous et al., 2010; Bottino, Capannelli and Comite, 2002; Genne, Kuyperes and Leysen, 1996), and ZnO (Shen et al., 2012). Many of these studies are summarized in Table 3.

Table 3: Summary of sources that have studied the impact of inorganic nanoparticles on membrane antifouling performance

	TiO2			ZrO2	SiO2		ZnO
Source	Jing-Feng Li et al. 2008	Jian-Hua Li et al. 2008	Wu et al. 2008	Maximous et al. 2009	Shen et al. 2011	Huang et al. 2012	Shen et al. 2012
Anti-fouling ability	Enhanced	Enhanced	Enhanced to optimal value	Enhanced to optimal value	Enhanced to optimal value	Enhanced to optimal value	Enhanced to optimal value
Hydrophilicity	Enhanced	Enhanced	Enhanced	Enhanced	Enhanced	Enhanced to optimal value	
Polymer material	PES	SMA/PVDF	PES	PES	PES		PES

Of these nanoparticles, TiO_2 has been studied the most thoroughly due to its stability, availability, (Wu et al., 2008) high hydrophilicity, and photocatalytic potential (Li et al., 2009). Jing-Feng Li et al. (2008) dispersed varying concentrations of TiO_2 nanoparticles (0-5 wt %) in polyethersulfone (PES) casting solutions and prepared composite membranes via phase inversion. They found that the composite membranes had enhanced thermal stability, hydrophilicity, and permeation performance. They recommended an optimal loading rate of 1-2 wt % TiO_2. Wu et al. (2008) also prepared TiO_2/PES composite membranes via nanoparticle dispersion and phase inversion. They

confirmed Jing-Feng Li et al.'s findings that the addition of TiO_2 enhanced the hydrophilicity, thermal stability, and mechanical strength of the membrane. However, they recommended an optimal TiO_2 loading rate of 0.5 wt % rather than 1-2 wt %. Jian-Hua Li et al. (2008) modified poly (styrene-alt-maleic anhydride)/poly(vinylidene fluoride) (SMA/PVDF) to contain TiO_2 nanoparticles via the self-assembly method. They also confirmed that the modified membranes had enhanced hydrophilicity and superior permeability.

SiO_2, though not as widely studied as TiO_2, has also been analyzed. Shen et al. (2011) prepared PES/SiO_2 composite membranes (0-5 wt % SiO_2) by the phase inversion method. They found that pure and raw water flux increased, hydrophilicity was enhanced, and anti-fouling ability increased with the addition of SiO_2. Huang et al. (2012) prepared mesoporous silica (MS) modified PES membranes via phase inversion. They found that the MS improved membrane hydrophilicity, porosity, anti-fouling ability, and thermal stability. They recommend an optimal MS loading rate of 2 wt %.

A third nanoparticle that has been studied for membrane modification is ZrO_2. Maximous et al. (2010) prepared PES/ZrO_2 composite membranes (0, 0.01, 0.03, 0.05, 0.07, and 0.1 PES/ZrO_2 weight ratios) via phase inversion and used these membranes for activated sludge filtration to study their fouling characteristics. They found that the addition of ZrO_2 particles improved mechanical strength and anti-fouling ability. They recommend an optimal ZrO_2 loading rate of 0.05 ZrO_2/PES. Two older studies (Bottino, Capannelli, and Comite, 2002; Genne, Kuypers and Leysen, 1996) also prepared ZrO_2 composite membranes. Though their analyses were not as thorough as those conducted by Maximous et al., both confirmed that permeability increased with the addition of ZrO_2.

Though less studied than the three other aforementioned particles, ZnO's effect on membrane performance has also been analyzed. Shen et al. (2012) prepared PES/ZnO composite membrane via phase inversion. They found that the addition of ZnO improves hydrophilicity, thermal decomposition temperature, water flux, and porosity.

All these experiments suggest that modifying membrane surfaces with TiO_2, SiO_2, ZrO_2 and ZnO both improves membrane hydrophilicity and enhances membrane antifouling performance. However, no study has compared which of these inorganic nanoparticles is most effective. Therefore, in this study, these inorganic nanoparticles were compared. To do this, five types of membrane were prepared. One of these membranes was not modified with inorganic nanoparticles, and the other four were each modified with either TiO_2, SiO_2, ZrO_2 and ZnO. The following section explains the processes used to prepare these membranes.

Membrane Preparation

Synthetic membranes have two primary types of structures: symmetric and asymmetric. Figure 11 demonstrates the difference between these structures. In symmetric membranes, the diameter of the pores is nearly constant throughout the entire cross section. Conversely, in asymmetric membranes, the pore size is not constant throughout the entire cross section. Instead, the

membrane contains two distinct layers, the top and bottom. The top layer is dense and governs the permeation properties of the membrane. The bottom layer is porous and simply provides mechanical support. In industry, most membranes used have an asymmetric structure (Matsuura, 1994).

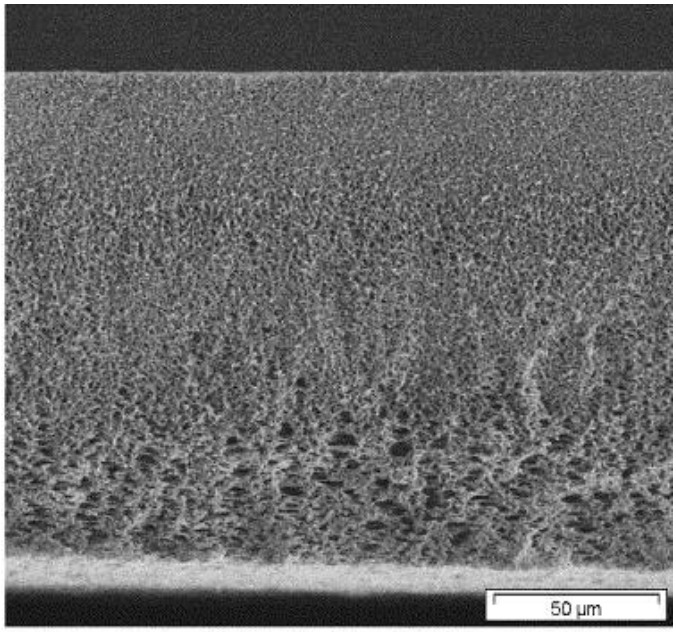

(a)

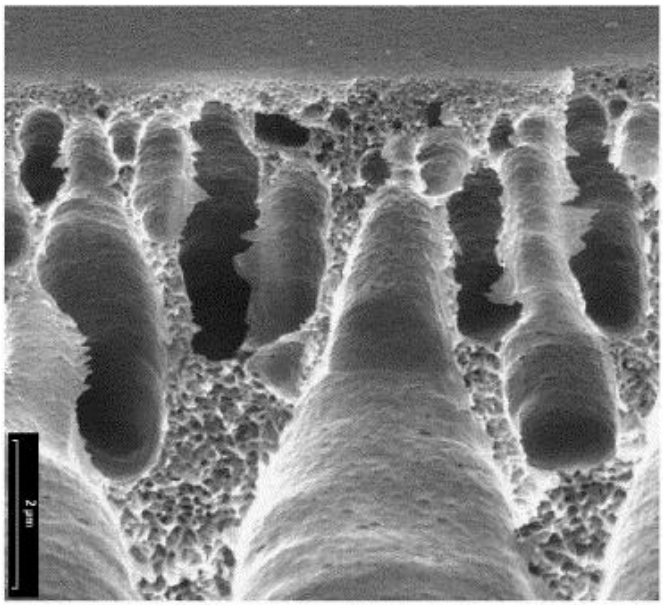

(b)

Figure 11: Demonstrates two different types of membrane strucutres, symmetric and asymmetric. (a) is symmetric, as the pores are all nearly equal in size. (b) is asymmetric, as it consists of two distinct layers (Membrane Structure).

Many methods have been developed to prepare asymmetric membranes (Matsura, 1994). Of these methods, phase inversion techniques are most commonly used.

Phase Inversion

Kools and Catherina (1998) explain that there are three ways to induce phase inversion: temperature induced phase inversion, reaction induced phase inversion, and dry-wet phase inversion. Of these, dry-wet phase inversion, or the *Loeb-Sourirajan* technique, is most common, and this was the technique used in this experiment.

For the *Loeb-Sourirajan* technique, a polymer solution is prepared by mixing a polymer and a solvent. This solution is than cast on a glass plate, and this plate is immersed into a *gelation bath.* The process involves two desolvation steps. First, when the solution is cast onto the glass plate, the solvent evaporates. This facilitates the formation of a thick skin layer at the top of the membrane. And second, when the solution is immersed into the *gelation bath*, solvent-nonsolvent exchange occurs. The nonsolvent diffuses into the polymer film while the solvent diffuses out. Due to these steps, the polymer solidifies into a porous membrane (ibid). Figure 12 illustrates this process:

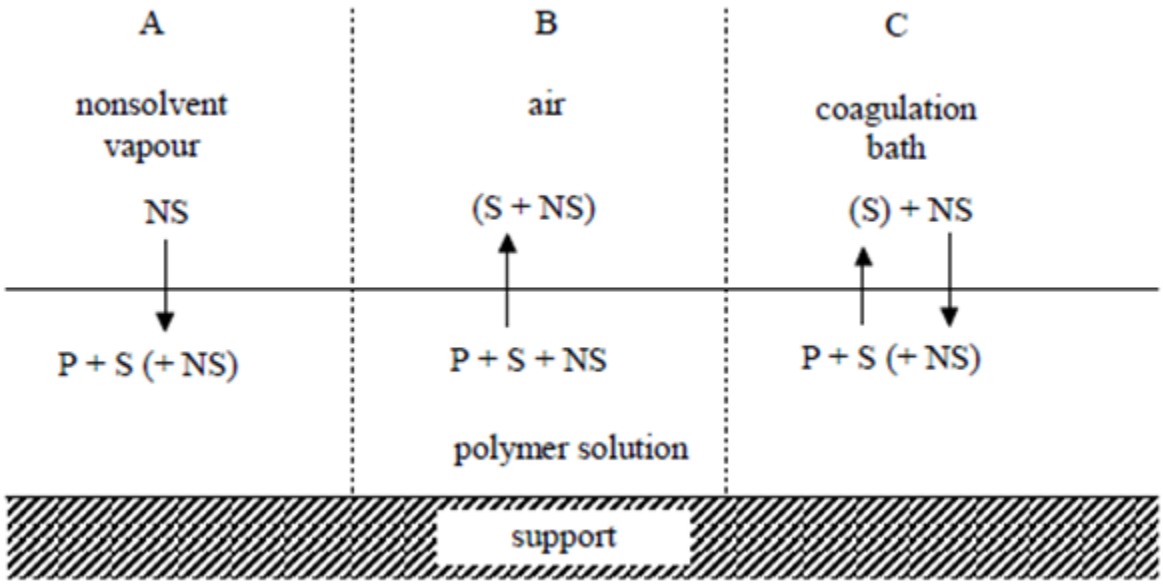

Figure 12: Schematic representation of three dry-wet separation processes. A) precipitation with nonsolvent vapor; B) evaporation of solvent; C) immersion precipitation. The arrows denote the net direction of diffusion for each step. Polymer, solvent, and nonsolvent are represented by P, S, and NS, respectively (Kools and Catherina, 1998).

For this experiment, the solvent used was dimethylacetmaide (DMAc), the nonsolvent was water, and the polymer was polyethersulfone. Figure 13 shows the ternary phase diagram for the phase inversion process in this experiment. The line with points A, B, C, and D denotes the path that the

membrane takes during this process. At point A, phase inversion has not begun, and the casting solution only consists of DMAc, PES, and additives. At point B, DMAc precipitates out and water molecules take its place. At point C, the membrane begins to solidify, and at point D, the process is complete. In total, phase inversion takes between 30 and 60 seconds (Saddat, 2011).

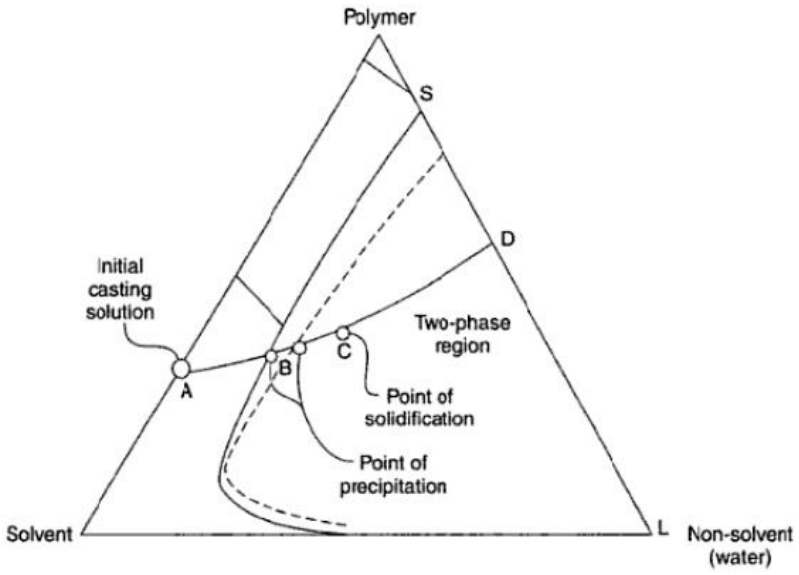

Figure 13: Ternary phase diagram for the phase inversion process through immersion precipitation (Matar, Hewitt and Ortiz, 1989)

It is important to note that, though this process is commonly used, it is not entirely understood. Due to the complex interplay between each component, "after thirty years of research in this field, many open questions still need to be answered." (Kools and Catherita, 1998)

Membrane Characterization

Following membrane preparation, numerous tests were done to characterize each membrane. A brief discussion about these tests and their value is below.

Viscosity

The viscosity of the casting solution was measured using a viscometer. The viscosity helps to predict the tensile strength of the membrane. High viscosities generally correlate with the formation of stronger membranes (Saddat, 2011).

Flux

Flux is defined by the volume of permeate that passes through a membrane per unit membrane surface area per unit time, as shown in Equation 1.

$$J = \frac{V}{A*t} \qquad \text{(Equation 1)}$$

Where J is equal to flux, V is volume of permeate, A is membrane surface area, and t is time.

Flux is an important indicator of membrane performance. Larger fluxes results in more rapid filtration and therefore reduced operating and implementation costs.

Porosity

Porosity is a measure of void space within a membrane. Porosity is calculated using Equation 2.

$$Porosity = \frac{Volume\ of\ Void\ Space}{Total\ Volume} * 100 \qquad \text{(Equation 2)}$$

The total volume of the membrane is determined through physical measurements. The volume of the void space is determined by comparing the mass of a membrane when it is wet and when it is dry. The difference between these masses is equal to the mass of water occupying the void space. Using the density of water, the volume of void space, then, can also be determined.

Porosity is important because it impacts flux.

Rejection Rate

Rejection rate measures how effectively a membrane can filter a particular pollutant. It is important because it dictates the quality of the permeate stream. Rejection rate is calculated using Equation 3.

$$Rejection\ Rate = \left(1 - \frac{C_p}{C_f}\right) * 100 \qquad \text{(Equation 3)}$$

Where C_p is the concentration of a particular component in the permeate stream, and C_f is the concentration of that same component in the solution prior to filtration.

Scanning Electron Microscope

A Scanning electron microscope (SEM) scans samples with focused beams of electrons. These electrons "interact with electrons in the sample" being studied, thereby producing information about the structure of the sample.

Images produced with a SEM elucidate the structure of particular membranes as well as the thickness of the surface layer of asymmetric membranes.

Fourier Transform Infrared Spectroscopy

Fourier transform infrared spectroscopy (FTIR) is used to obtain the infrared spectrum of for a particular sample. It collects data over a wide spectral range, and this data can be used to identify specific functional groups that are present in the sample being studied.

For this experiment, FTIR was used to determine whether or not specific inorganic nanoparticles were present on the surfaces of the prepared membranes.

X-ray Photoelectron Spectroscopy

X-ray photoelectron spectroscopy (XPS) is used to determine the elemental composition of the surface of a particular sample. XPS irradiates a material with X-rays and then measures the kinetic energy and number of electrons that escape the surface of the sample being analyzed. This data

can be used to determine the elements that are present on the sample surface. (Queen Mary University London)

Contact Angle

Contact angle is the measurement of the angle at which a liquid/vapor interface meets a solid surface. For this experiment, contact was used to determine the relative hydrophilicity of membrane surfaces. Contact angles greater than 90 degrees indicate hydrophobicity, and contact angles less than 90 degress indicate hydrophilicity. Therefore, low contact angles are preferable to high ones (Agrawal).

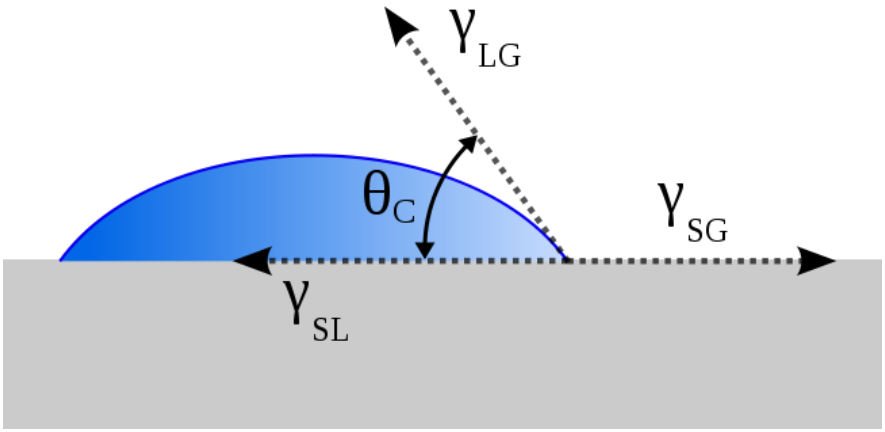

Figure 14: Illustration of contact angle (http://en.wikipedia.org/wiki/File:Contact_angle.svg)

Atomic Force Microscopy

Atomic force microscopy (AFM) is used to analyze the surface of membrane samples. Information is gathered with sharp tip on the end of a cantilever. This tip scans the membrane surface, and forces between the tip and the membrane surface "lead to a deflection of the cantilever according to Hooke's Law." This process yields valuable data about membrane surface, and it can be used to render three dimensional images of the surface as well as to measure characteristics such as surface roughness and pore size distribution.

Section Summary

In summary, membranes are complex. There are numerous factors that impact their performance, and there are numerous tests used to characterize membranes. This knowledge will be applied to analyze the membranes prepared in this experiment.

Methodology

In this experiment, five distinct membranes were prepared: a pure PES membrane and four PES membranes that were modified with different inorganic nanoparticles (TiO_2, SiO_2, ZnO, and ZrO_2). Following membrane preparation, several tests were conducted to characterize membrane performance. This section discusses the methods used to both prepare and characterize the membranes.

Membrane Preparation

All five membranes were prepared using the phase inversion method. For the phase inversion method, the first step was to create a casting solution for each different membrane. However, before the casting solutions were prepared, the inorganic nanoparticles needed to be prepared. If added to the casting solution untreated, the inorganic nanoparticles would aggregate and the modified membranes would not have been as effective, according to Shen et al. (2011). Therefore, to increase their dispersability in the casting solution, the inorganic nanoparticles were treated according to the method described by Shen et al. (2011), the details of which are described in the section below.

Pre-treatment of inorganic nanoparticles

For each inorganic nanoparticles, 1000 mL of H_2O were measured into two beakers. The pH of each of these beakers was then lowered to 4.0, and a 3.5 weight percent sodium dodecyl sulfate (SDS) solution was then created with this water. 5 g of inorganic nanoparticles were then added to each 1000 mL solution, and the solution was then stirred for 8 hours. Following this stirring, the solution was then vacuum filtered so as to isolate the inorganic nanoparticles. The isolated nanoparticles were then vacuum dried for 8 hours at 60 degrees C to remove any remaining water. After drying, the particles were ready for addition to the casting solutions.

Casting solution preparation

After treating the inorganic nanoparticles, the casting solutions were then ready to be prepared. In total, five casting solutions were created, one for each membrane that was tested. Each casting solution consisted of dimethylacetamide (DMAc) as the solvent, pure PES, and the additive polyethylene glycol 400 (PEG 400). The casting solutions for the modified membranes also contained inorganic nanoparticles. Figure 15 shows the weight percentages of each component for the pure PES membrane casting solution, and Figure 16 shows the weight percentages of each component for the modified membranes' casting solutions. Tables 9-13 in Appendix 2 show the mass of each component that was present in each casting solution.

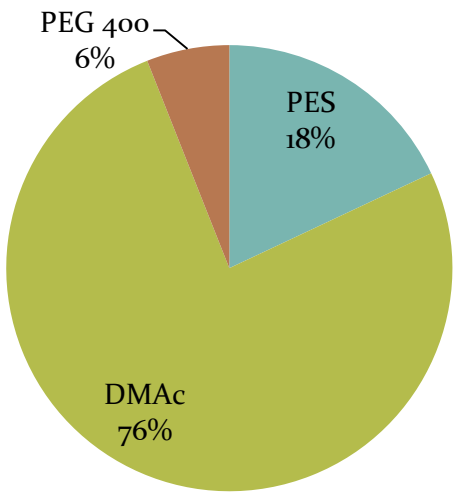

Figure 15: Weight percentages of the components of the pure PES membrane

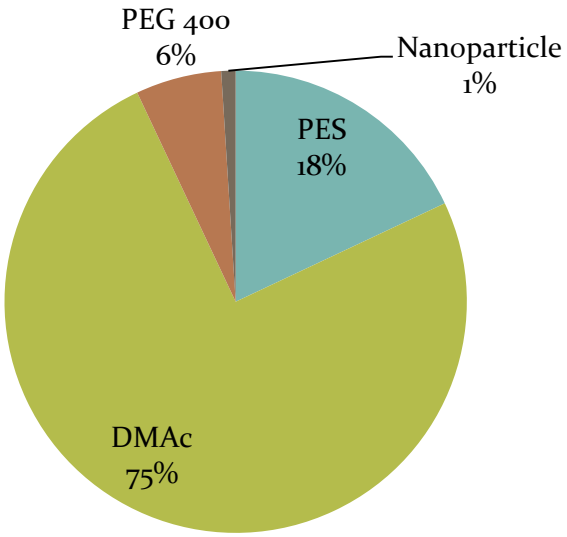

Figure 16: Weight percentages of the components of the four modified PES membranes

To prepare the pure PES casting solution, half of the necessary DMAc was first added to a 500 mL flask. The PES was then added in small increments with regular mixing. After all the PES was added, the remaining DMAc and the PEG 400 were then added as well. The solution was then stirred in a water batch heater at 60 degrees C for 6-8 hours, or until all the PES had dissolved. After stirring, the solution was then allowed to sit for at least 24 hours so as to eliminate all bubbles.

To prepare the PES/inorganic nanoparticle casting solutions, half of the necessary DMAc was first added to a 500 mL flask. The flask was then placed in a high speed stirring machine, and, little by little, inorganic nanoparticles were added. After all the inorganic nanoparticles were added, the solution was stirred for an additional ten minutes. After this stirring, the PES was then added incrementally with regular mixing. After all the PES was added, the remaining DMAc and the PEG 400 were then added as well. The solution was then stirred in a water batch heater at 60 degrees C for 6-8 hours, or until all the PES had dissolved.

Figure 17 is an image of three of the completed casting solutions.

Figure 17: Three of the completed casting solutions

Following the preparation of all five casting solutions, the viscosity of each casting solution was then measured. After taking the viscosity measurements, membranes were then able to be prepared.

Casting the Membranes

To create the membranes, the newly-prepared casting solutions were poured onto a glass plate, and a machine evenly distributed the casting solutions across this plate. The machine was set to a particular thickness so that the thickness of all the prepared membranes would be as equal as

possible. Figure 18 is an image of the glass plates that the casting solution is poured on, and Figure 19 is an image of the machine that evenly distributes the casting solutions across these plates.

Figure 18: The glass plates that the casting solutions are poured onto

Figure 19: This machine evenly distributes the casting solutions across the glass plates at a specified thickness

After the casting solution was evenly distributed across the glass plate, it was exposed to the air for 30 seconds. After this 30 seconds, the plate was then dipped into distilled water where it remained for two minutes. The distilled water (which is replaced for each new membrane) induced the phase inversion process, and this was the point in the procedure when the membrane was actually formed. After two minutes, the newly-formed membrane was removed from the water where it was placed in another container with pure water. It sat in this container for 24 hours, after which it was ready to be characterized.

Membrane Characterization

After all the membranes were prepared, they were characterized. Numerous characterization tests were conducted over the course of this experiment. Some were conducted by me, while others were conducted in other laboratories. A summary of all the characterization tests is provided in Table 4.

Table 4: Summary of tests used to characterize prepared membranes

Conducted by me	Conducted by others
Pure Water Flux	Fourier Transform Infrared Spectroscopy
Resistance	X-ray Photoelectron Spectroscopy
Rejection Rate	Atomic Force Microscopy
Flux Decline	Scanning Electron Microscope
Flux Recovery	Breaking Force
Zeta Potential	Elongation Rate
Porosity	Total Gravimetric Analysis
	Contact Angle

In this section, the methodology for the tests that I conducted will be described.

Pure water flux

After the membranes were prepared, the pure water flux at 0.03, 0.05, 0.07, 0.09, and 0.1 MPa was measured for each. When the pressure was adjusted, at least 20 minutes passed before flux measurements were taken. This allowed the membrane to reach a steady state flux. Once at least 20 minutes passed, the time it took to filter 40 g of water through each membrane was recorded. From this data, the pure water flux was calculated at each different pressure.

Resistance

To calculate the intrinsic membrane resistance (R_m), the pure water flux data was graphed on a curve (pure water flux versus pressure), and a linear curve was fit to this data. R_m was calculated from this curve.

Rejection rate

To determine the rejection rate, a 1000 mg/L BSA solution was filtered through each membrane. However, before this filtration occurred, the BSA solution needed to be prepared, and a concentration curve needed to be created. The concentration curve allowed us to determine the concentration of BSA in the permeate stream by calculating its absorbance.

BSA Concentration Curve

To create the BSA concentration curve, six solutions of BSA were created, all with different concentrations of BSA (10, 100, 200, 400, 700, and 1000 mg/L BSA). The absorbance for each of these pre-made solutions was calculated, and a graph was then created with absorbance data on the y-axis and BSA concentration data on the x-axis. A linear curve was then fit to this data. With this linear curve, the concentration of BSA could be determined with absorbance data.

After the BSA concentration curve was created, the 1000 mg/L BSA solution was filtered through each membrane. The absorbance of the permeate stream was then calculated, and this absorbance data was used to calculate the BSA concentration in the permeate stream. From this, rejection rate for each of the membranes was determined.

Flux decline

To determine flux decline, again, a 1000 mg/L BSA solution was filtered through each membrane. The permeate stream was diverted into a beaker, and the mass of this beaker was measured every 10 seconds. All this data was recorded by a computer and was later exported into Microsoft Excel. Using Microsoft Excel, it was determined how the mass flow rate changed with time. From this, it was determined how the flux changed with time, which in turn elucidated how much the flux was reduced and how long it took for a steady state flux to be reached.

Flux recovery

After the flux decline experiments were finished, pure water was filtered through each of the membranes, and a new pure water flux was determined.

Following the determination of this new pure water flux, each membrane underwent a series of cleaning procedures. First, the membrane was cleaned with pure water. This was accomplished by placing the membrane in a beaker of water and shaking the beaker for twenty minutes. After this cleaning was finished, the pure water flux was measured again.

After the pure water cleaning, the membrane was cleaned with NaOH. This was accomplished by letting the membrane sit in an NaOH solution for twenty minutes. After the NaOH cleaning, the pure water flux was taken again.

After the NaOH cleaning, the membrane was then cleaned with NaOCl. Again, to accomplish this, the membrane was placed in an NaOCl solution where it remained for twenty minutes. After this twenty minutes was complete, the pure water flux was measured again.

After all the cleanings were complete, the new pure water fluxes measured after cleaning were compared to the pure water fluxes before cleaning. From this data, the flux recovery ratio was determined.

Porosity

To calculate the membrane porosity, the volume of a membrane sample was first determined. Next, the weight of this membrane sample was calculated when wet. After this, the membrane was dried for 8 hours at 60 degrees C, and the dry weight was then measured. From all this data, the porosity of the membrane was determined. This was repeated for three sample for each different membrane, and the values for each sample were averaged together.

Results & Discussion

The first tests conducted on the membranes were FTIR and XPS. Both these tests can help to determine the chemical composition of a particular sample. Therefore, they were used to confirm that the prepared membranes contained the chemicals they were supposed to contain. The results of these tests are shown below.

FTIR

The FTIR results are shown in Figure 20. In this Figure, each colored line corresponds to a different membrane. As shown, it is clear that all the membranes contain very similar functional groups, as they all have very similar peaks. This is expected because the chemical compositions of the membranes are nearly exactly the same.

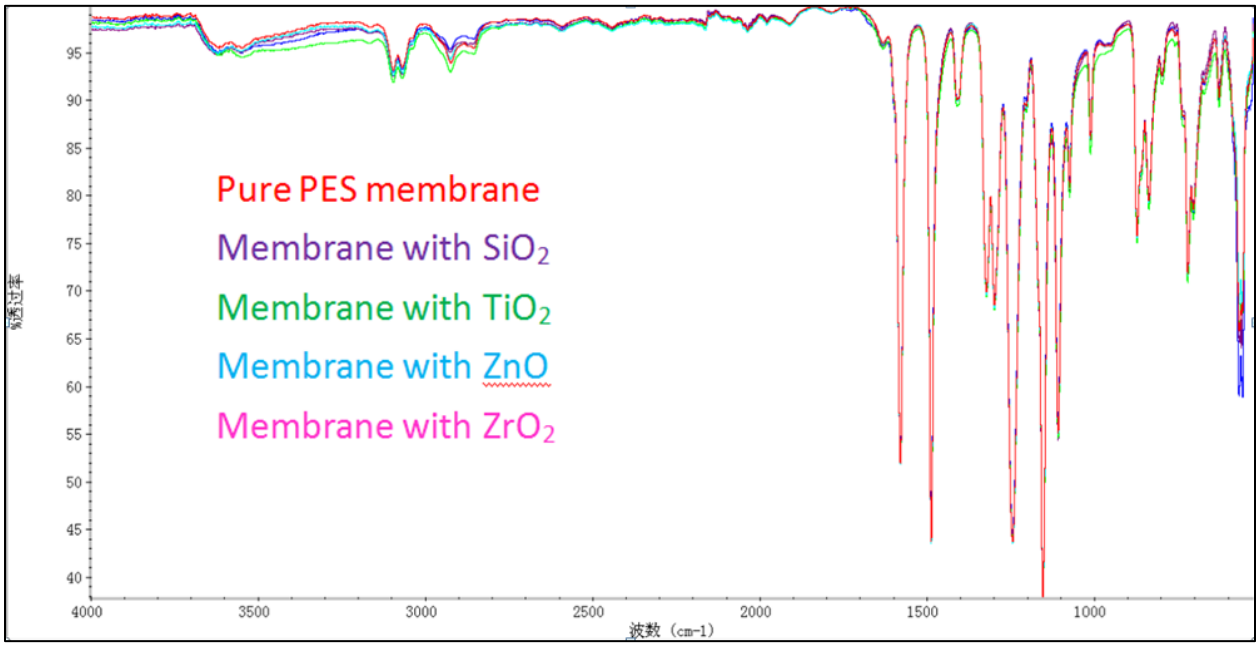

Figure 20: Fourier transform infrared spectroscopy results. The different peaks correspond to different organic functional groups. Each colored line corresponds to a different membrane.

Table 5 presents the results from the analysis of the FTIR data. Several peaks were identified, and functional groups that correspond to these peaks were then identified as well. From this analysis, it was clear that DMAc, PEG 400, and PES were all present in each of the membranes. Unfortunately, inorganic nanoparticles were not detected using this method because the weight percentages of these nanoparticles were all too small.

Table 5: Summary of the results from the FTIR tests

Organic compound	Wave number(cm^{-1})	Functional group
DMAC	1579.36	C=O
	1244.43	C-N
PEG400	1153.00	$-CH_2-$
	1107.40	$-CH_2-$
PES	900~700	para-benzene
	1500~1300	OCH_3-benzene

XPS

Because FTIR could not detect the inorganic nanoparticles in the modified membranes, XPS was used. A summary of the XPS data for all five membranes is shown in Figure 21. As is clear, like the data for the FTIR, the data for XPS for all five membranes are also very similar. This, again, is because the elemental compositions for each of the membranes are very similar.

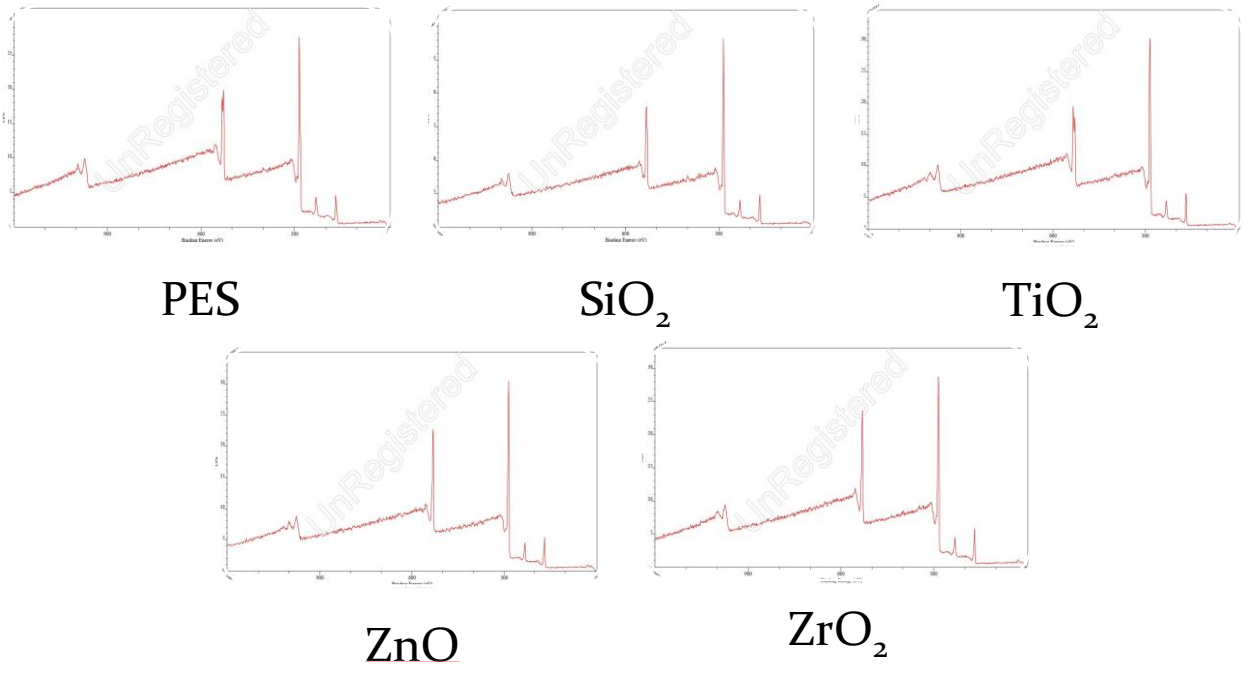

Figure 21: Summary of XPS data for all five membranes

However, this general data was further analyzed to determine whether eight elements – oxygen, carbon, nitrogen, sulfur, silicon, titanium, zinc, and zirconium – were present in each sample. The results for each of these analyses are shown in Figures 22-25. Each figure compares the results from one modified membrane to the results from the pure PES membrane. In each case, the inorganic nanoparticle that was supposed to be present in the modified membrane was present. However, this inorganic nanoparticle was never present in the modified membrane. This indicates

that the methodology used succeeded in embedding inorganic nanoparticles on the membrane surface.

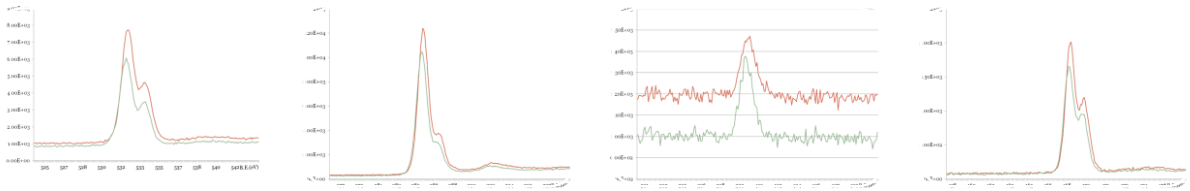

Oxygen Carbon Nitrogen Sulfur

Si

Figure 22: Comparison of the XPS results for the SiO_2 modified membrane and the pure PES membrane. The red lines correspond to the data for the SiO_2 membrane, and the blue lines correspond to the data for the pure PES membranes. As is clear, each membrane contained oxygen, carbon, nitrogen, and sulfur. However, only the SiO_2 modified membrane contained silicon, as expected.

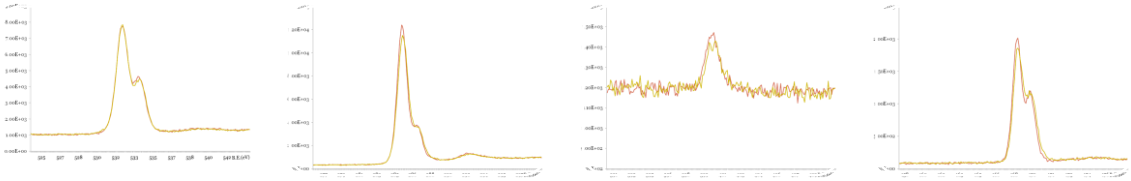

Oxygen Carbon Nitrogen Sulfur

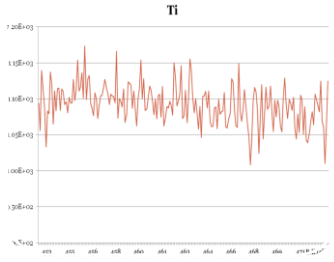

Ti

Figure 23: Comparison of the XPS results for the TiO_2 modified membrane and the pure PES membrane. The red lines correspond to the data for the TiO_2 membrane, and the gold lines correspond to the data for the pure PES membranes. As is clear, each membrane contained oxygen, carbon, nitrogen, and sulfur. However, only the TiO_2 modified membrane contained titanium, as expected.

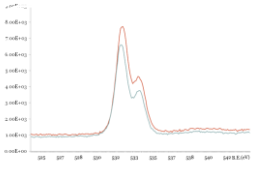

Oxygen

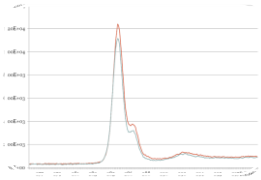

Carbon

Nitrogen

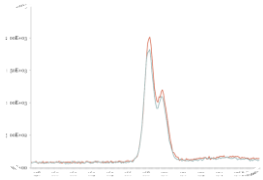

Sulfur

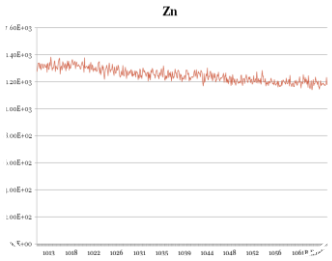

Zn

Figure 24: Comparison of the XPS results for the ZnO modified membrane and the pure PES membrane. The red lines correspond to the data for the ZnO membrane, and the blue lines correspond to the data for the pure PES membranes. As is clear, each membrane contained oxygen, carbon, nitrogen, and sulfur. However, only the ZnO modified membrane contained zinc, as expected.

ZrO_2

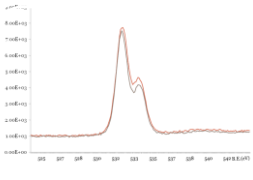

Oxygen

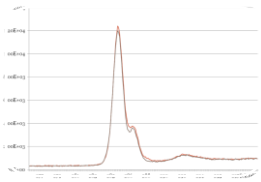

Carbon

Nitrogen

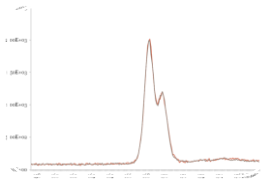

Sulfur

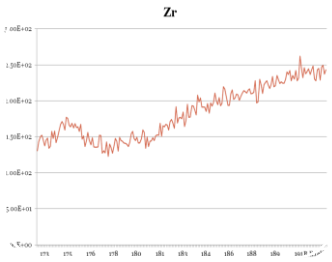

Zr

Figure 25: Comparison of the XPS results for the ZnO modified membrane and the pure PES membrane. The red lines correspond to the data for the ZnO membrane, and the purple lines correspond to the data for the pure PES membranes. As is clear, each membrane contained oxygen, carbon, nitrogen, and sulfur. However, only the ZrO_2 modified membrane contained zirconium, as expected.

Hydrophilicity

After XPS and FTIR demonstrated that the methodology used was successful – each membrane that was prepared contained the proper chemicals and inorganic nanoparticles – the next step was to determine membrane hydrophilicity. Theoretically, modified membranes should be more hydrophilic. The reason for this is because the inorganic nanoparticles used are polar molecules. Water is also a polar molecule, so therefore the two should attract each other. Since the nanoparticles are on the membrane surface, by attracting water towards them, they make the surface more hydrophilic. Figure 26 illustrates this phenomenon.

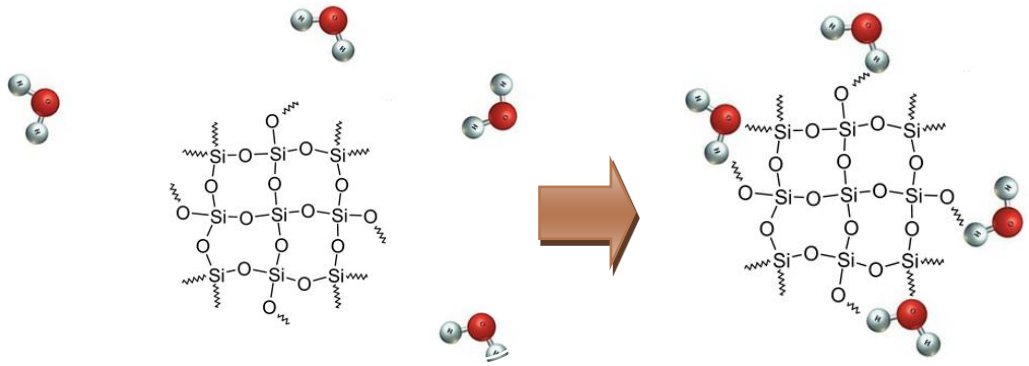

Figure 26: This image shows amorphous SiO_2 and water molecules. Because both are polar, the two attract each other. The silicon image was taken from http://upload.wikimedia.org/wikipedia/commons/8/8b/SiO2.svg. The water molecule image was taken from http://image.tutorvista.com/cms/images/44/molecular-geometry-of-water.JPG.

Contact Angle

To determine the relative hydrophilicity of the prepared membranes, their contact angles were tested. A small contact angle indicates greater hydrophilicity whereas a large contact angle indicates greater hydrophobicity. The results of this analysis are presented in Figure 27.

As expected, the pure PES membrane had the greatest contact angle indicating that it was the most hydrophobic. This suggests that the inorganic nanoparticles successfully did improve membrane hydrophilicity.

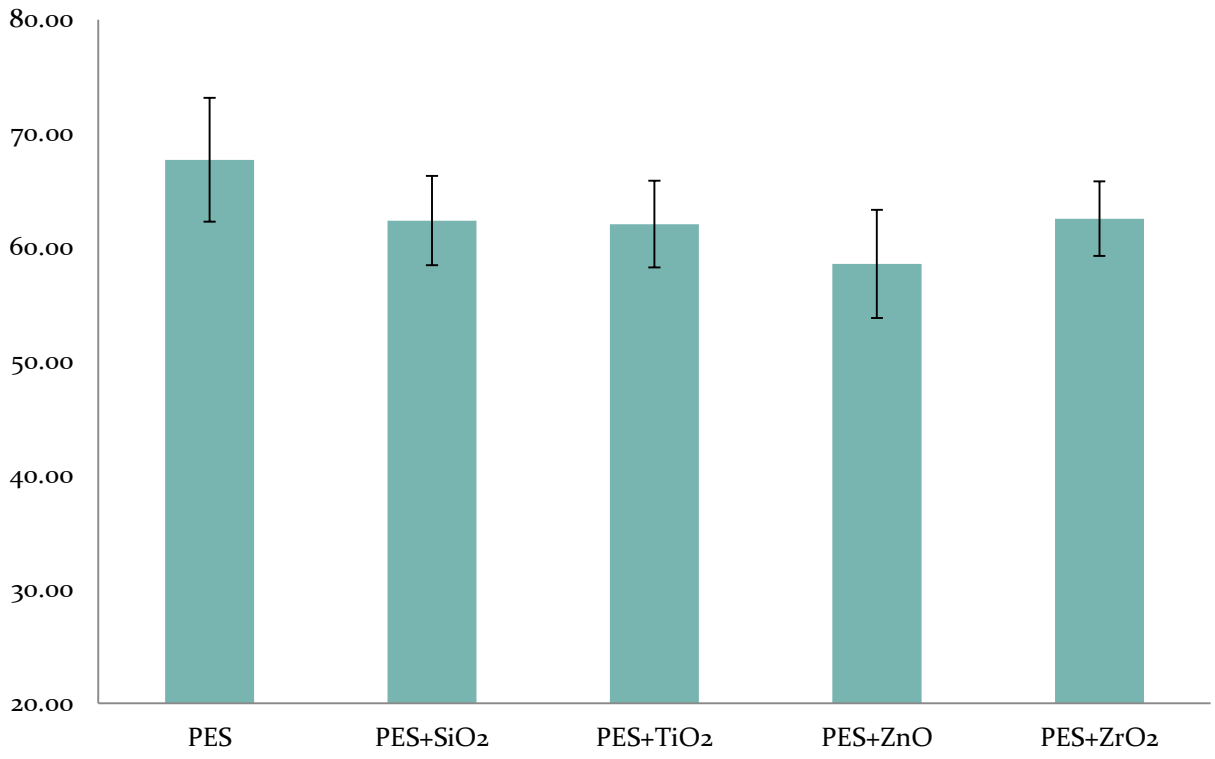

Figure 27: Contact angles of each of the prepared membranes. PES had the largest contact angle followed by ZrO_2, SiO_2, TiO_2, and ZnO.

Figure 28 compares each of the modified membranes. It illustrates the reduction of each membrane's contact angle relative to the contact angle of the pure PES membrane. ZnO showed the greatest reduction in contact angle (13.5%), followed by TiO_2 (8.3%), SiO_2 (7.9%), and ZrO_2 (7.6%). These results indicate that ZnO was the most hydrophilic of the five prepared membranes.

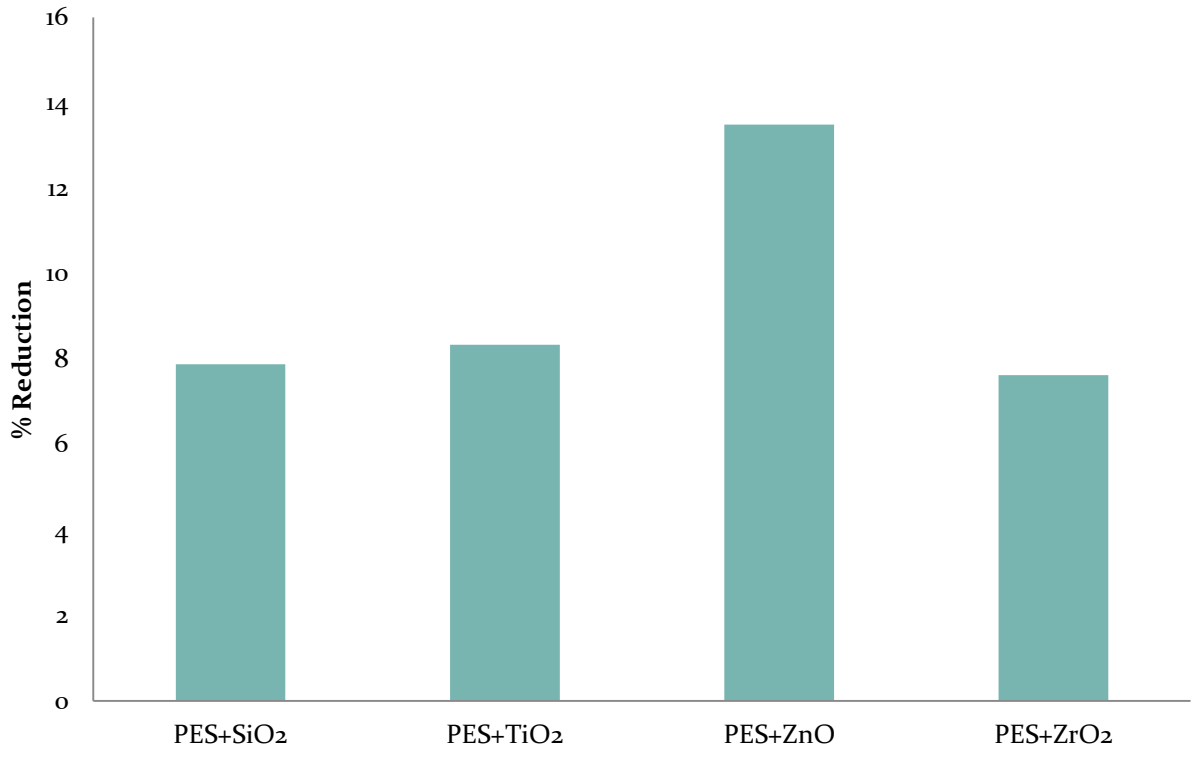

Figure 28: Reduction in the contact angle of the four modified membranes as compared to the pure PES membrane. The ZnO membrane showed the greatest contact angle reduction, followed by TiO_2, SiO_2, and then ZrO_2.

Antifouling Performance

After determining that the contact angles for each of the modified membranes had been reduced by the inorganic nanoparticles, the next step was to determine if this reduction in contact angle led to enhanced antifouling performance. To accomplish this, flux reduction curves were generated from the BSA filtration data (see "Flux Decline" section in methodology for more details). These curves are presented in Figure 29. All these curves correspond well with theory. Each shows three distinct phases of fouling, as described by Marshall, Munro and Tragardh (1993). The first, which is rapid, occurs in the first minute and is the result of concentration polarization. The second, which reduces flux at a moderate rate and lasts significantly longer than the first phase (up to seven hours in the case of this experiment), is caused by protein deposition on the membrane surface. And the third phase is where the curves flatten and the flux remains nearly constant (Marshall, Munro and Tragardh, 1993).

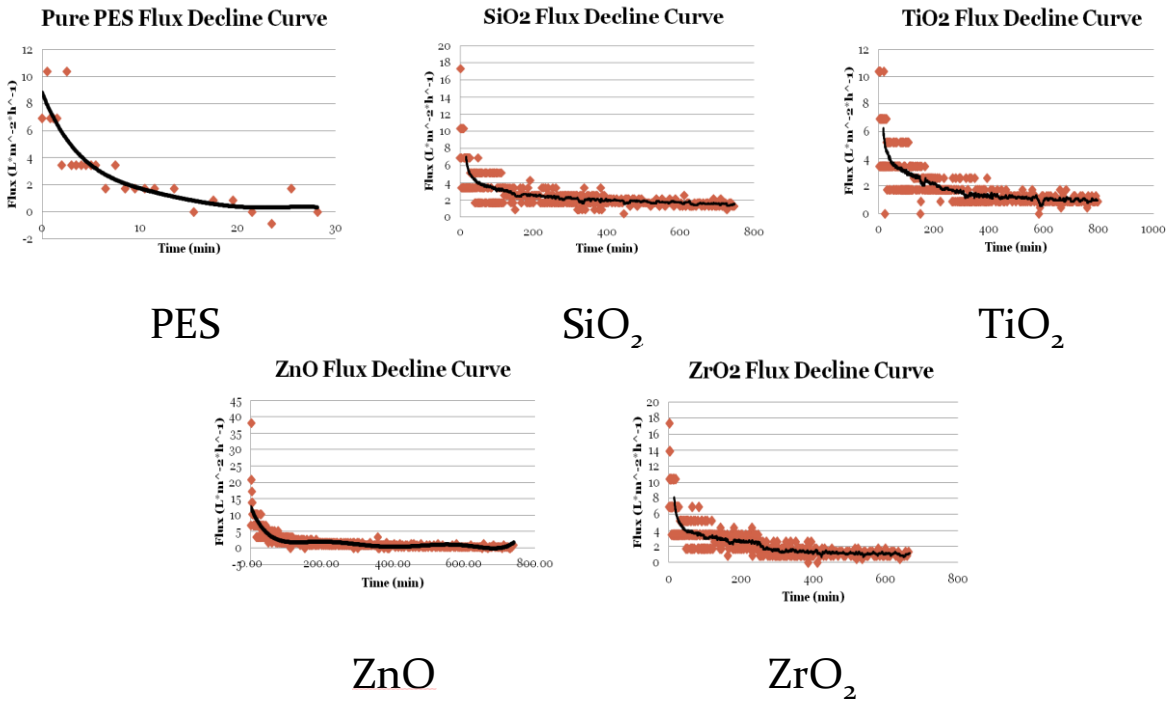

Figure 29: Flux decline curves for all five prepared membranes. On the x-axis is flux (L/m^2*hr), and on the x-axis is the time when the flux measurement was taken (minutes). The longer it takes for the graph to plateau, the better the antifouling performance.

The time it takes for the third phase to be reached is indicative of anti-fouling performance. The longer it takes to reach the third phase, the more time it took for proteins to form a monolayer on the membrane surface. Therefore, the membrane that takes the longest to reach the third phase is the least likely to foul.

Figure 30 illustrates the time it took each membrane to reach the third phase. Of all the membranes, PES took the least amount of time, by far (~20 minutes), to reach this phase. This indicates that the pure PES membrane fouled the most easily, which, in turn, indicates that the addition of the inorganic nanoparticles did enhance membrane anti-fouling performance, as expected.

ZnO, surprisingly, took the second least amount of time to reach the third phase of flux reduction (~200 minutes), which indicates that it fouled the second most easily. This was unexpected because it showed the greatest reduction in hydrophilicity, which should enhance antifouling performance. This suggests that factors other than membrane hydrophilicity, like porosity, roughness, and pore distribution, also affect membrane anti-fouling performance, and some of these factors will be discussed later in the paper to explain why the ZnO-modified membrane's antifouling performance was improved the least. SiO2 and TiO2 both took the longest to reach phase three (~400 minutes), which indicates that they had they had the best anti-fouling performance.

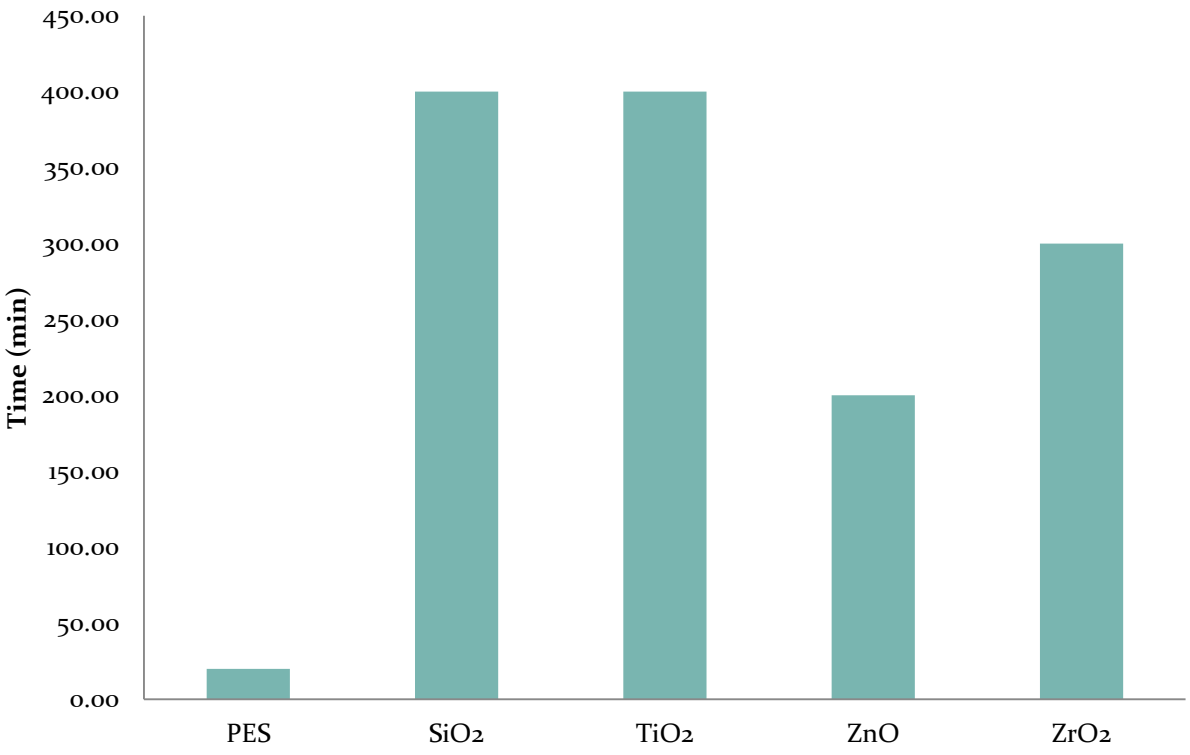

Figure 30: Illustrates the amount of time it took each membrane to reach a constant flux. The pure PES membrane took the shortest amount of time, followed by ZnO, ZrO2, and then SiO2 and TiO2.

After generating flux decline curves, the pure water flux of the membranes was recorded. After this pure water flux was recorded, the membranes were cleaned with pure water, and the pure water flux was taken again. These tests allowed flux recovery ratios to be calculated for each membrane, and the results from these tests are shown in Figures 31 and 32.

Figure 31 shows the percent of the original flux that was attained after cleaning with pure water. The higher percentage, the smaller the reduction in initial pure water flux. The ZnO membrane came closest to its original flux, indicating that fouling affected it the least (relative to its original flux).

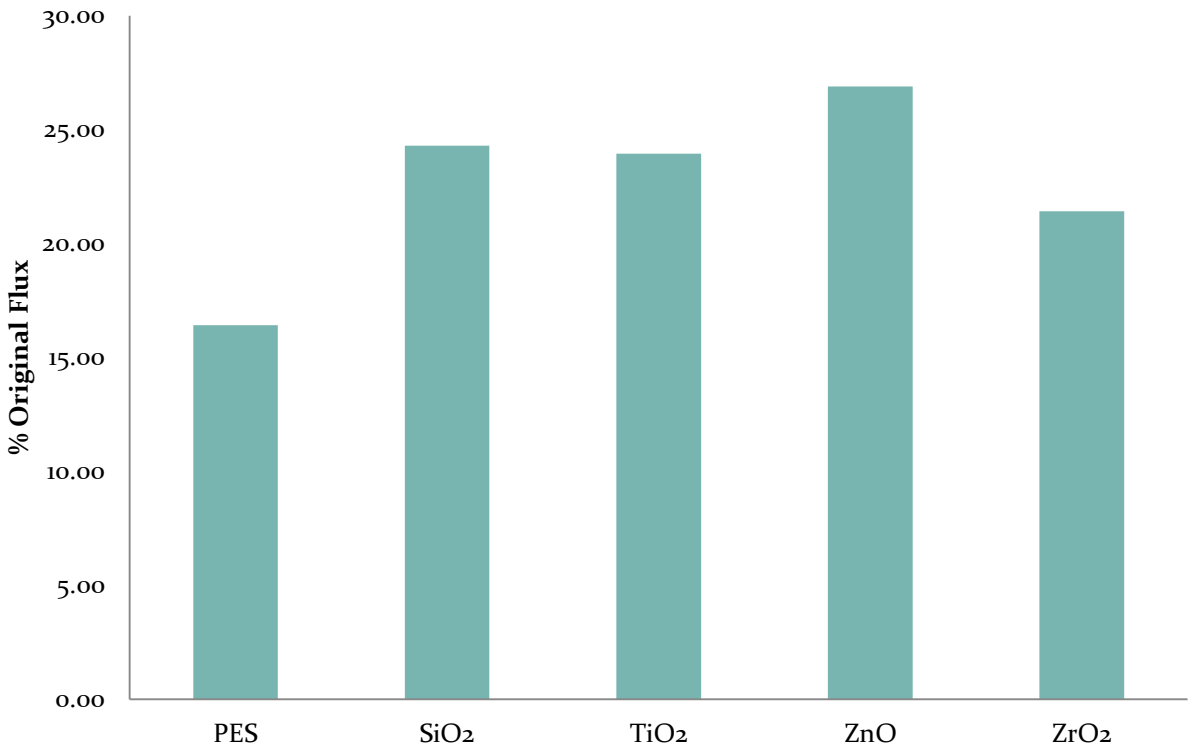

Figure 31: % of initial pure water flux recovered after the membranes were cleaned with pure water. ZnO showed the greatest original flux recovery followed by SiO_2, TiO_2, ZrO_2, and PES

Figure 32 compares the pure water flux directly after BSA filtration to the pure water flux after membrane cleaning. It shows how much, in percent, the pure water flux of each membrane improved after cleaning. The higher the percentage, the greater the anti-fouling performance, as a higher percentage suggests that foulants were easily removed by water rinsing and therefore adhered less strongly to the membrane surface. SiO_2 by far showed the greatest flux recovery in this test. Therefore, SiO_2 performed the best in terms of anti-fouling performance, as it was the most resistant to membrane fouling in each test. The pure PES membrane recovered the least amount of flux, which, again, was expected because its surface was the most hydrophobic.

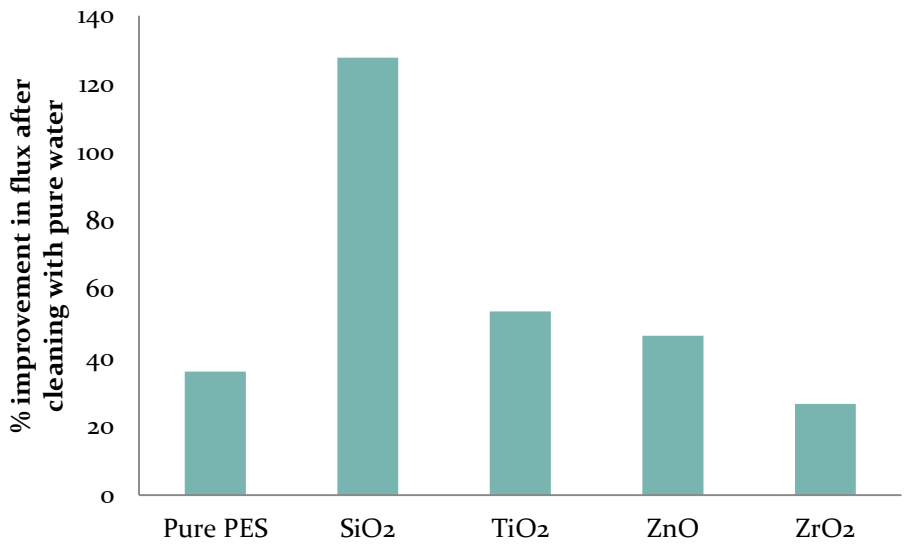

Figure 32: Percent improvement in flux after cleaning with pure water of all five prepared membranes

Summary of Membrane Antifouling Performance

The introduction of inorganic nanoparticles reduced the hydrophilicity of PES membranes. The ZnO's hydrophilicty was reduced the most followed by TiO_2's, SiO_2's, and ZrO_2's. TiO_2 and SiO_2 took the longest to reach the third stage of flux decline, indicating that they were most resistant to membrane fouling, and both also showed the greatest improvement in flux when they were cleaned with pure water after BSA filtration. However, ZnO came closest to its original pure water flux after being cleaned with pure water, and SiO_2 demonstrated the greatest improvement in flux after being cleaned. The pure PES membrane performed the worst in all these experiments.

Based on these tests, SiO_2 demonstrated the best antifouling performance. It took the longest to foul and it demonstrated, by a significant margin, the greatest flux improvement after it was cleaned.

Pure Water Flux

Though anti-fouling performance is important, other membrane characteristics are important as well. Initial pure water flux, for example, must be considered. The original pure water flux of each of the membranes is shown in Figure 33. The pure PES membrane had the lowest pure water flux, suggesting that the addition of inorganic nanoparticles no only enhanced membrane anti-fouling performance, but also flux. This is partly because the inorganic nanoparticles are polar and therefore attract polar water molecules to the membrane surface, thereby improving pure water flux. Of the modified membranes, ZnO had the smallest initial pure water flux. Therefore, even though it showed the greatest recovery in original flux (Figure 31), this does not mean it is the best membrane. SiO_2 demonstrated the greatest initial pure water flux.

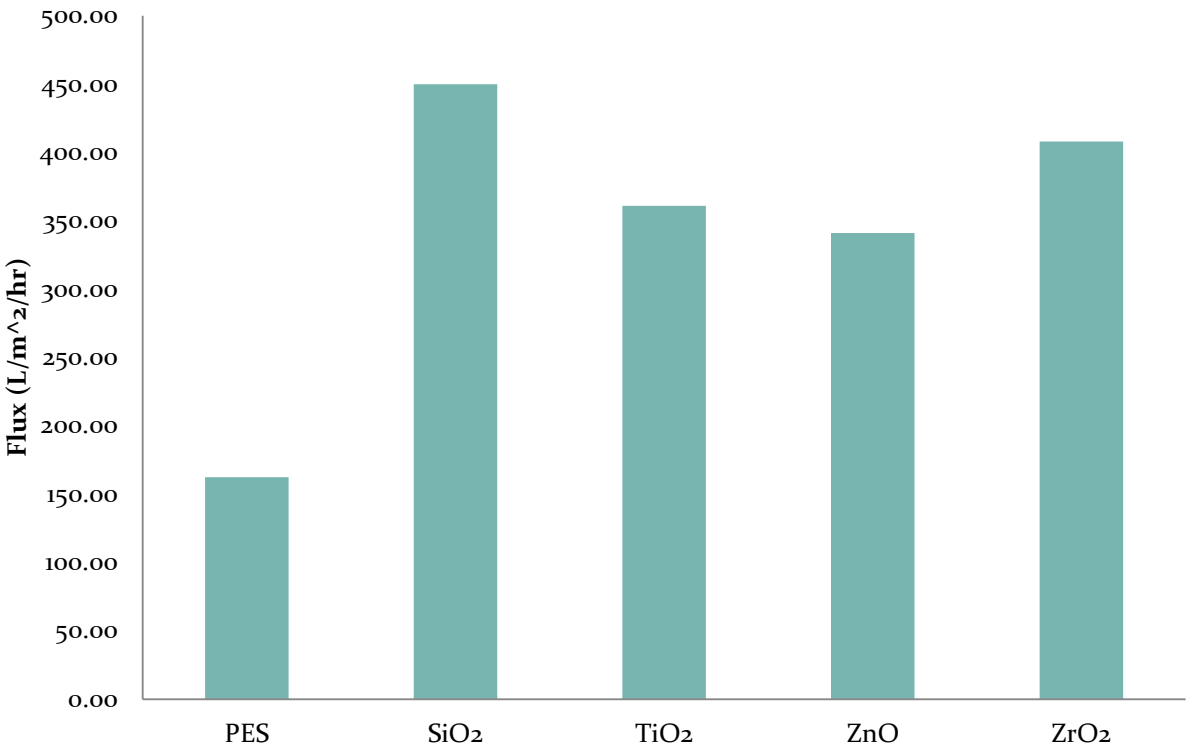

Figure 33: Initial pure water flux prior to filtration with the BSA wastewater.

Rejection Rate

Rejection rate is an important parameter as well. Even if a membrane has excellent anti-fouling performance, if it cannot purify wastewater adequately, it cannot be used. Rejection rate data for BSA are presented in Figure 34. As shown, most of the membranes have similar rejection rates, with the SiO_2 membrane performing the best by a small margin. However, the TiO_2 membrane is noticeably lower than that of the other four membranes. As a result, even though the TiO_2 membrane has performed well on the antifouling tests, it may not be suitable for applications that require high levels of purification.

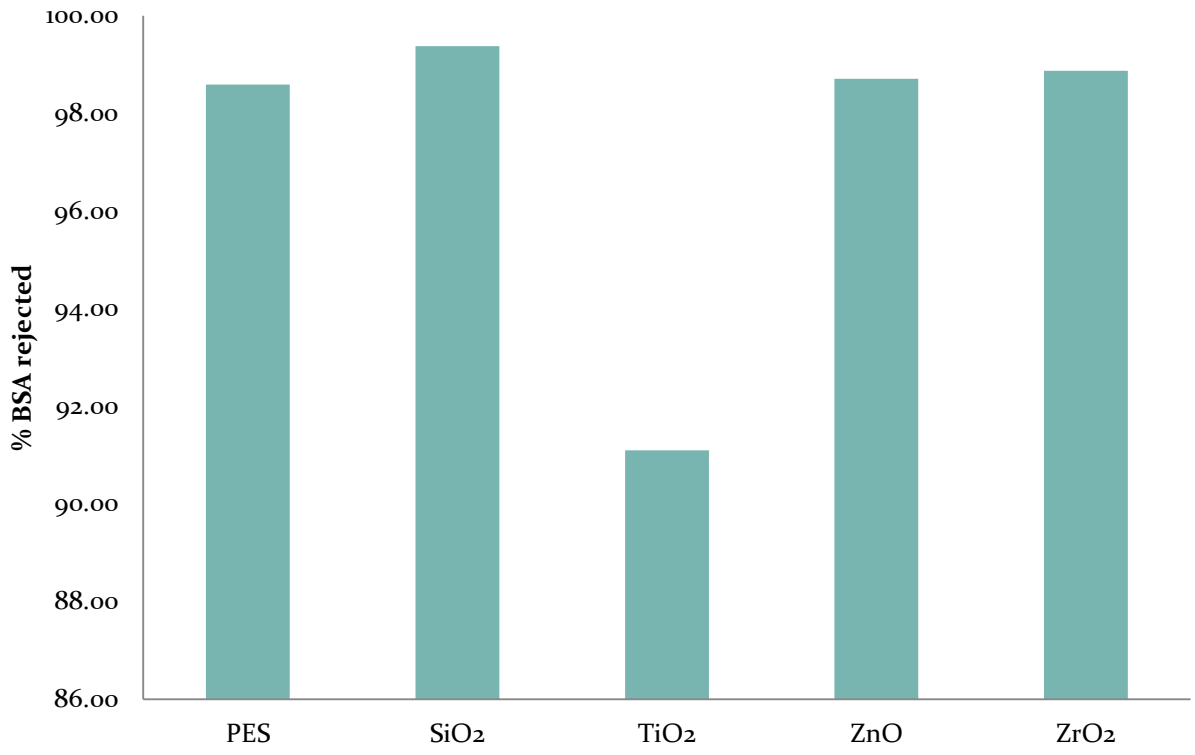

Figure 34: Rejection rate of all five prepared membranes

Porosity

The results from the porosity tests are shown in Figure 35. The porosity in all the modified membranes is smaller than the pure PES membrane. Of the modified membranes, SiO_2 exhibited the smallest porosity, whereas ZrO_2 exhibited the largest. This does not correspond to literature results

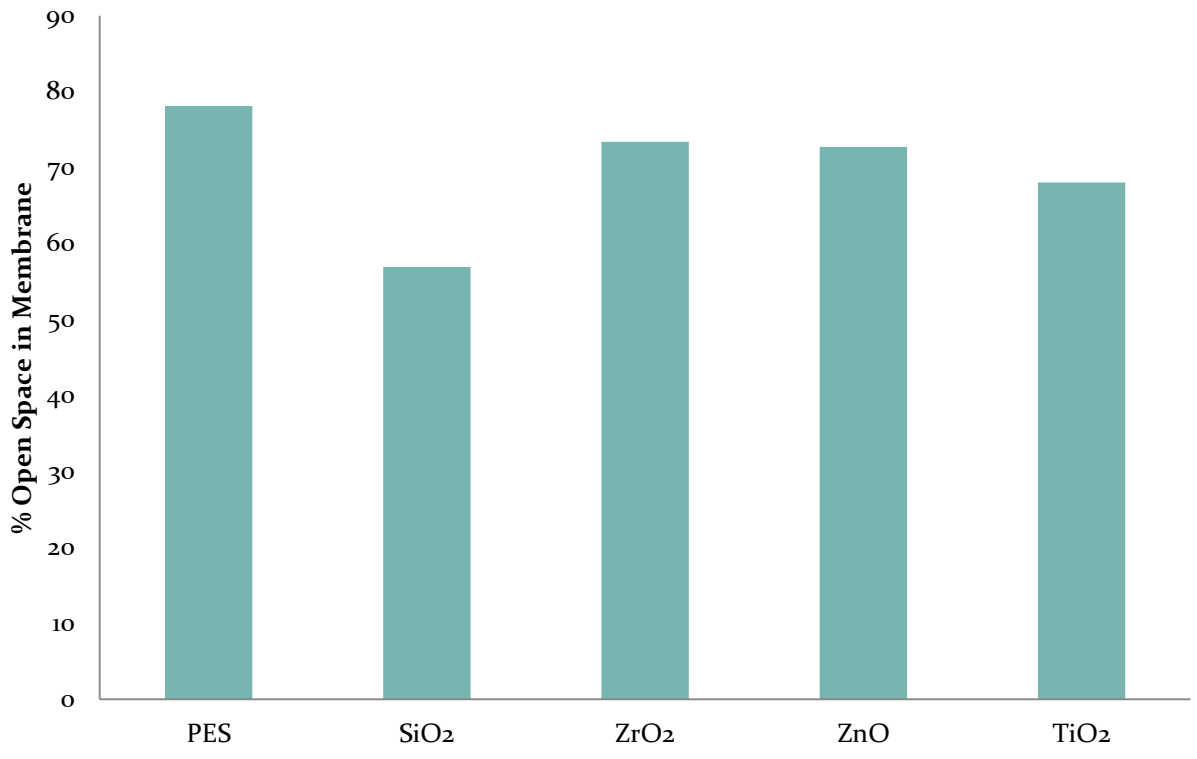

Figure 35: Porosity of all five prepared membranes

According to Cuperus and Smolders (1991), low porosity generally results in greater fouling. They write that low surface porosity can "aggravate the effect of adsorption and fouling" due to the build-up of solute near the membrane pores. By increasing porosity, solute will accumulate more evenly across the membrane surface. Strangely, despite having the lowest porosity, SiO_2 fouled the least. This may because the porosity measured was not simply surface porosity, but porosity for the membrane as a whole. Also, hydrophilicity could impact membrane anti-fouling performance greater than porosity.

Roughness

The surface roughness values for each of the membranes are shown in Figure 36. As is clear, the pure PES membrane had the largest surface roughness (129.47 µm), and the SiO_2 membrane had the lowest surface roughness (21.69 µm). Of the modified membranes, the ZnO membrane had the highest surface roughness (87.83 µm)

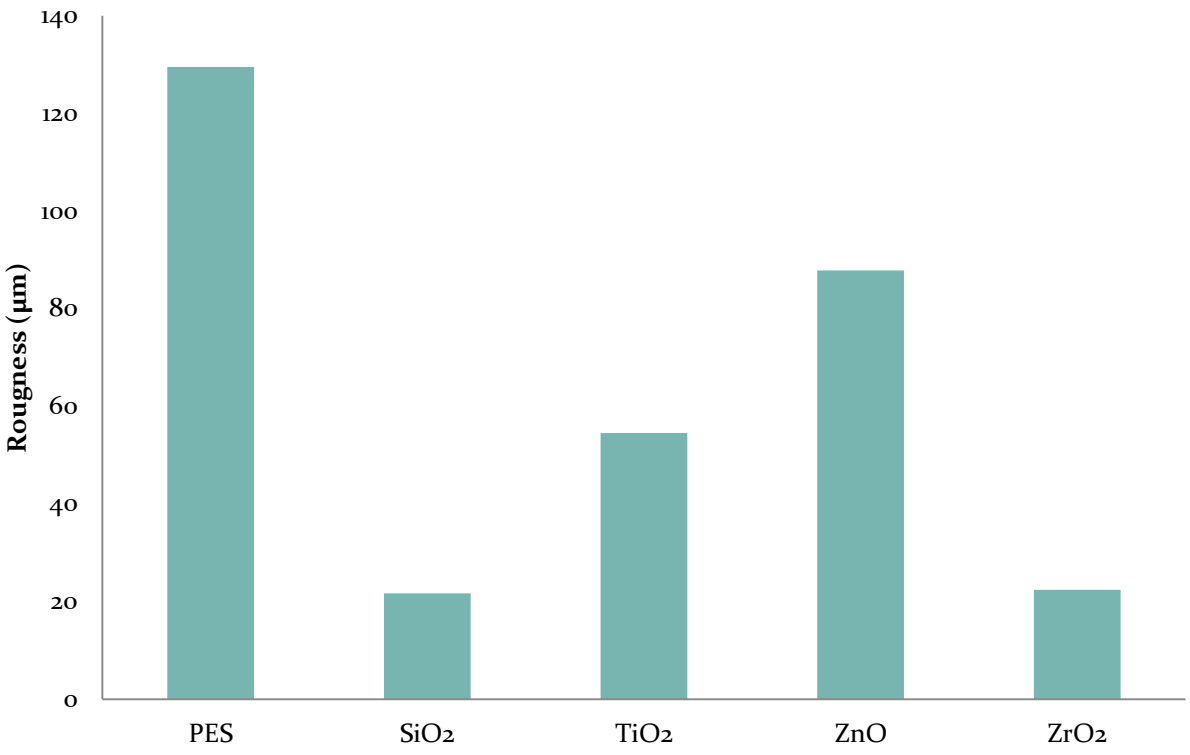

Figure 36: Roughness values for all five prepared membranes

Greater roughness often results in greater fouling (Cuperus and Smolders, 1991). Greater surface roughness leads to greater surface area, which creates more opportunities for solute adsorption. Also, greater roughness "deteriorates" the hydrodynamics near the surface, which in turn exacerbates concentration polarization as well as fouling. (Cuperus and Smolders, 1991).

Because of this, it is not surprising that the SiO_2 membrane had the lowest surface roughness value, as it was the least susceptible to fouling. Likewise, it is also not surprising that, of the modified membranes, the ZnO membrane had the highest surface roughness value, as it was the most susceptible to membrane fouling. *Surface roughness, then, could explain why, though the ZnO membrane was the most hydrophilic, it did not display the best anti-fouling performance.*

Mechanical Properties

Mechanical properties of membranes are important to consider as well, and the mechanical properties of the prepared membranes are shown below. Figure 37 displays the elongation rates of all five prepared membranes. As is clear, the PES membrane had the best elongation rate, as it was higher than the four other modified membranes.

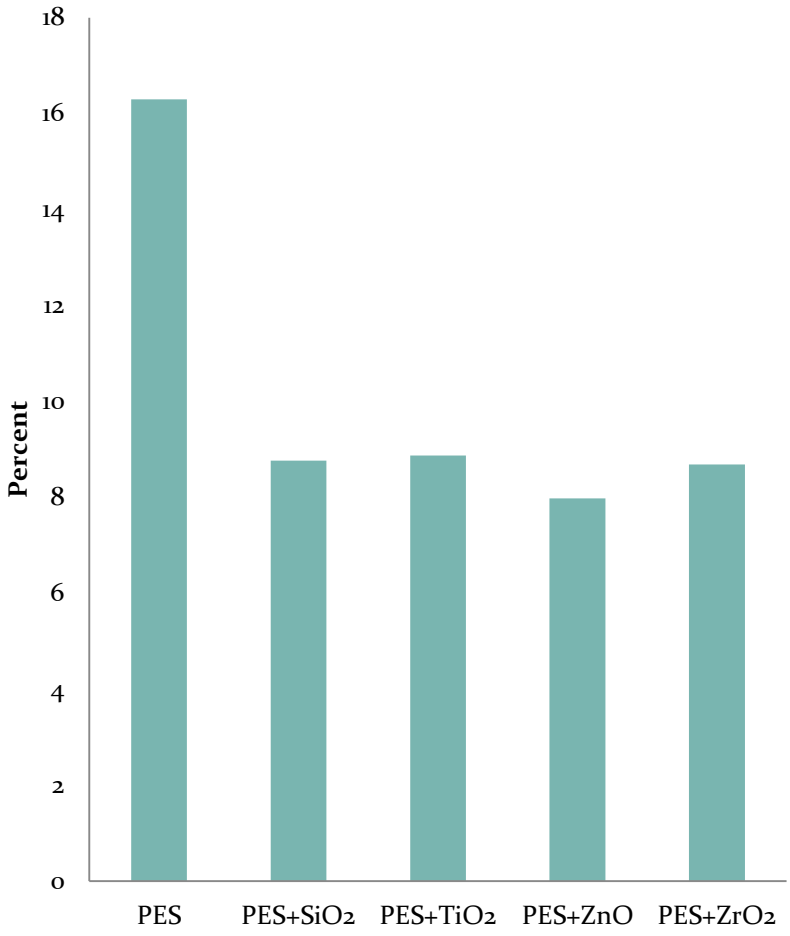

Figure 37: Elongation rate of the five prepared membranes

Figure 38 displays the breaking force of all five prepared membranes. Again, as is clear, the PES membrane had the best breaking force, as it was higher than the four other modified membranes.

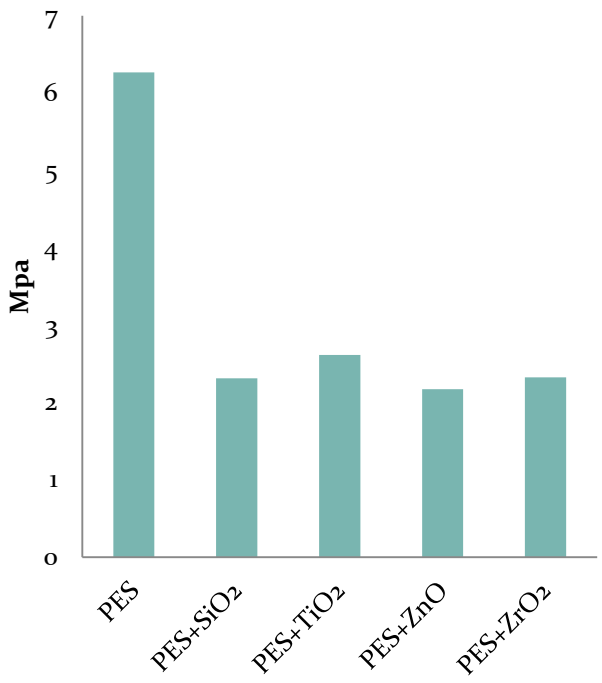

Figure 38: Breaking force of the five prepared membranes

These two mechanical tests, breaking force and elongation rate, indicate that the modified membranes all had poorer mechanical properties than the pure PES membrane. This was not an expected result, as the literature suggests that the mechanical properties of organic polymer membranes generally improve with the addition of inorganic nanoparticles (Wu et al. 2008). Wu et al. explain that, if the inorganic nanoparticles are evenly distributed throughout the membrane, they serve as "cross-linkages" to bear the stress of the membrane load. However, these authors also note that nanoparticle aggregation can lead to reduced mechanical properties, so it is possible that nanoparticles aggregated in the modified membranes prepared for this experiment.

Thermal Properties

Like mechanical properties, thermal properties are important to consider as well, especially if the membranes will be used for high-temperature applications. Figure 39 shows the glass transition temperature of all five prepared membranes. The pure PES membrane demonstrated the best glass transition temperature, as it was the highest of the five. Again, this was unexpected, as the literature suggests that the addition of inorganic nanoparticles to organic polymer membranes should enhance the thermal properties (Huang et al. 2012, Shen et al. 2011). Wu et al. explain that the inorganic nanoparticles absorb heat, and therefore the membranes' thermal properties should improve. It is unclear why the thermal properties decreased in this experiment.

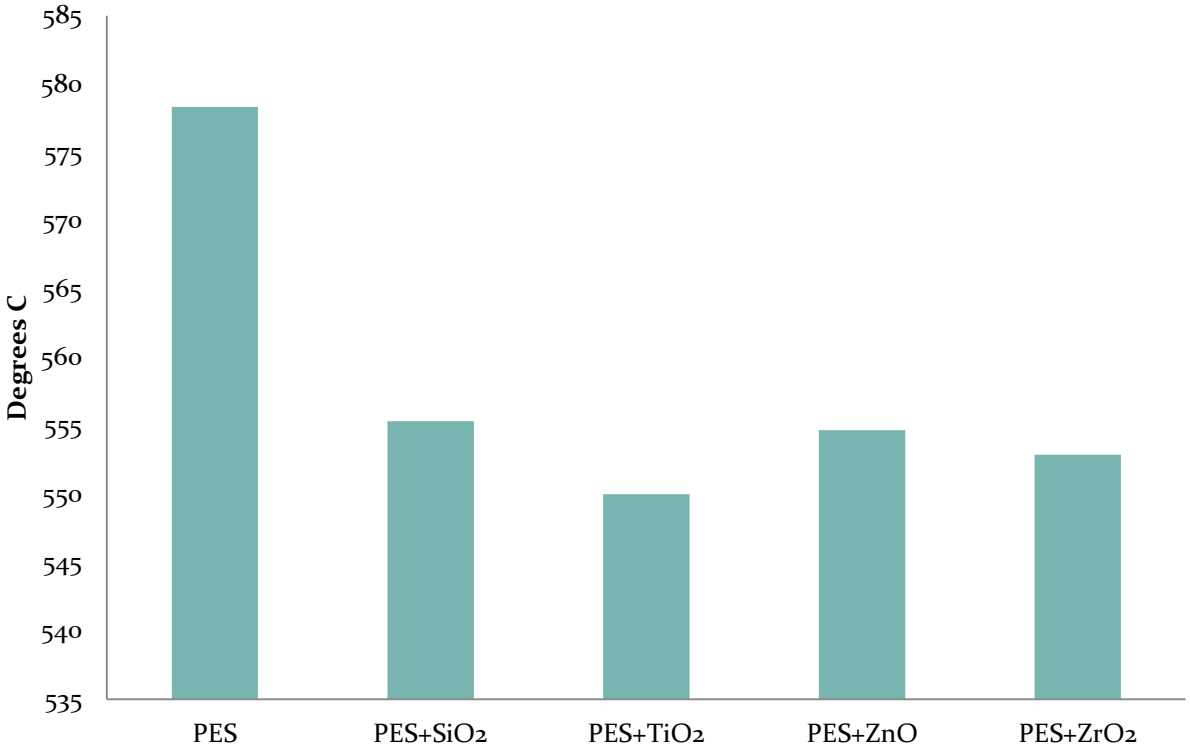

Figure 39: Glass transition temperatures of the five prepared membranes.

SEM

A SEM was used to analyze the morphology of all five prepared membranes. The results below show SEM images for both the membrane cross section and the membrane bottom surface.

Cross Section

Figure 40 shows the SEM image of the cross section of the membranes at a scale of 100 micrometers. As can be seen in the images, all membranes exhibit an asymmetric structure with a thick skin layer. However, it is also clear that the nanoparticles significantly affected the morphology of the PES membrane below the thick skin layer. For the pure PES membrane, the structure is reasonably consistent, finger-like, and spongy. For the modified membranes, though, the structure is less consistent, does not contain finger-like pores, and does contain large void spaces. These void spaces could explain why the mechanical properties of the modified membranes were not as good as the mechanical properties of the pure PES membrane.

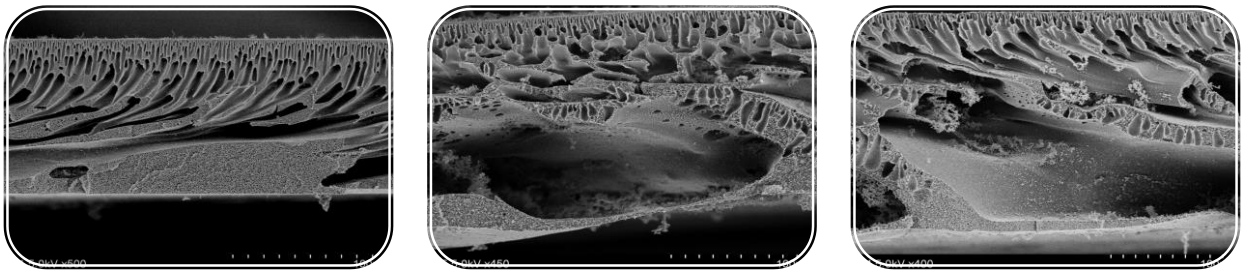

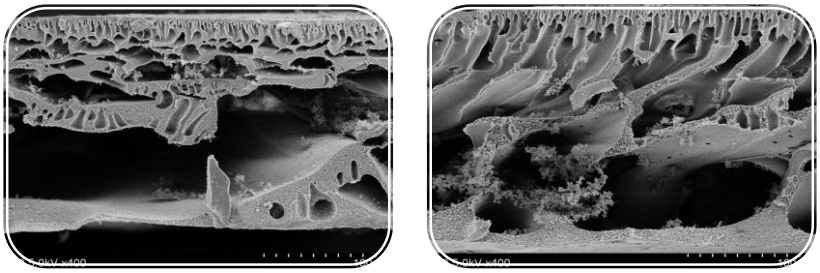

Figure 40: Cross sectional SEM image of the five prepared membranes at a scale of 100 micrometers

The literature reports mixed results for the effect of inorganic nanoparticles on membrane morphology. Huang et al. (2012) report that pure and modified membranes (SiO_2/PES) display similar morphologies – morphologies similar to that for the pure PES membrane. However, although similar to the pure PES membrane, they also note that the modified membranes contain fewer macrovoids, as the increased viscosity of the modified casting solutions delays the exchange rate between solvent and nonsolvent during the phase inversion process. Jiang-nan Shen et al., who also prepared SiO_2/PES membranes, reported similar results to those of Huang et al. – the modified and pure PES membranes had similar structures – but also observed increased connectivity between the pores in the sub- and bottom-layers for the modified membranes.

Unlike these studies, though, in preparing ZnO/PES membranes, Liguo Shen et al. (2011) found that the modified membranes did exhibit noticeable morphological differences when compared to the pure PES membrane. At low weight percentages (<2%), the modified membranes had a greater number of pores than the pure PES membrane. These results are more in line with the ones obtained in this experiment.

Wu et al. (2008) suggest a reason that large pores, like those observed by Liguo Shen et al., could have formed in the membrane sublayer. They studied PES/TiO_2 composite membranes and observed a "considerable" number of broken and collapsed pores near TiO_2 aggregates. These pores could have formed because of interfacial stresses between the polymer and the nanoparticle during the membrane drying process. If the membranes prepared in this experiment exhibited nanoparticle aggregation, this aggregation, then, could explain the existence of the observed

pores because it could have caused interfacial stresses. Again, these nanoparticle aggregation could be responsible for the diminished mechanical properties of the modified membranes.

Further research on the impact of nanoparticles on membrane morphology would be beneficial, as the literature reports conflicting results.

Bottom Surface

Figure 41 shows the SEM bottom surface images of the five prepared membranes at a scale of ten micrometers. As is clear, there are significantly more pores on the bottom surface of the modified membranes. This, again, is likely the result of nanoparticle aggregation. As explained in the last section, nanoparticle aggregates could have caused interfacial stresses that led to larger pores in the membrane sublayer. This phenomena is particularly evident in the image of the SiO_2 membrane.

5 micrometers

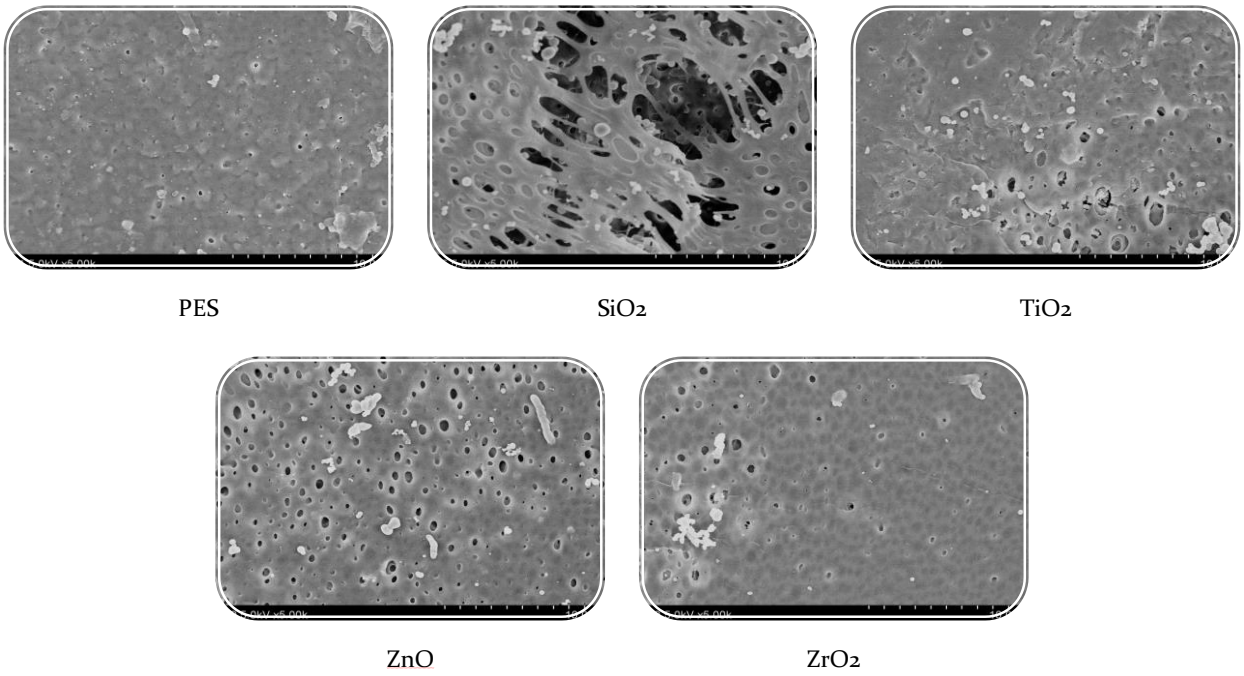

Figure 41: Bottom surface SEM image of the five prepared membranes at a scale of 10 micrometers

Summary

Table 6 summarizes many of the results from this experiment. Highlighted in red are the membranes that performed best in each particular experiment. Because of its high initial pure water flux, high rejection rate, and superior antifouling performance, the SiO_2 membrane performed best in this experiment. Therefore, of these nanoparticles, it is the recommended option.

Table 6: Summary of results. The boxes in red indicate the membrane that performed best in each particular category.

	Initial Pure Water Flux (L/m2/h)	Rejection Rate (%)	Roughness (µm)	Porosity (%)	Contact Angle	Reduction Contact Angle (%)	Approximate Time till Complete Fouling (min)	Flux Recovery after Pure Water Cleaning	Zeta Potential
PES	162.26	98.59	129.47 ± 36.46	78.10	67.69	0.00	20.00	16.42	1.69
SiO2	449.75	99.37	21.69 ± 2.77	56.92	62.36	7.87	400.00	24.29	1.43
TiO2	360.97	91.09	54.50 ± 36.79	73.38	62.05	8.33	400.00	23.94	0.53
ZnO	340.95	98.71	87.83 ± 84.16	72.71	58.56	13.49	200.00	26.89	0.48
ZrO2	407.91	98.87	22.37 ± 2.63	68.03	62.53	7.62	300.00	21.42	18.1

Recommendations

In general, it would be beneficial if research on inorganic nanoparticles and membrane performance was more systematized. There are numerous different tests, nanoparticles, and methodologies for preparing and characterizing these composite membranes. As a result, there is little consistency among experiments conducted in different laboratories, and there is little room for comparison among different studies. A comprehensive database where researchers from different labs could input their results according to different methodologies, nanoparticles, and wt % of nanoparticles, could help solve this problem. This database would also help to make clear the gaps in knowledge that currently exist and therefore could help to focus future research.

Regarding future research, there are still numerous experiments that could help improve understanding of the impact inorganic nanoparticles can have on antifouling performance. For example, in this experiment, the nanoparticles were only dispersed at 1 wt % in the membrane. Other wt %'s should be tested for all these nanoparticles. Also, due to time constraints, none of the tests in this experiment were run more than once. Therefore, the membranes prepared in this study need to be further studied. And last, cleaning methods need to be analyzed, different wastewaters need to be tested, and economic studies need to be conducted.

To summarize, though this study was one of the first to compare different nanoparticles in controlled experiments, there still remains significant gaps in knowledge that a more systemized research strategy would help to fill.

Treatment Facility Design

Introduction: Membrane Bioreactor

A waste water treatment facility will be designed based on the results from this experiment. The facility will use a membrane bioreactor to treat municipal wastewater. A membrane bioreactor (MBR) is unique because it combines a conventional activated sludge (CAS) system with membrane technology. Figure 42 illustrates the different processes involved in a membrane bioreactor system as well as the processes involved in a typical activated sludge system.

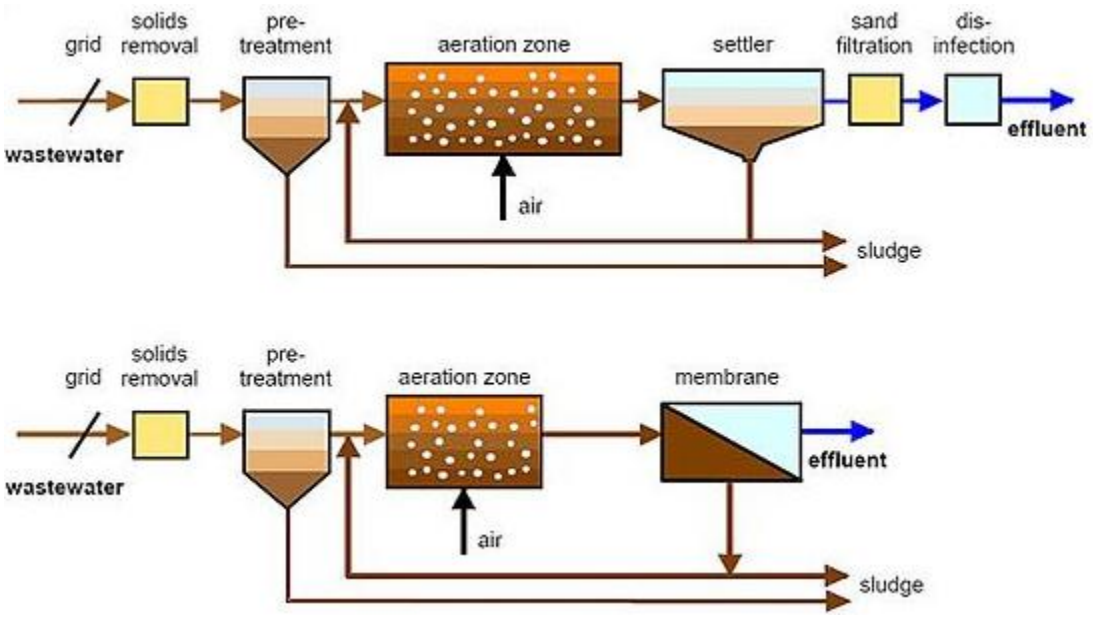

Figure 42: Schemactic of typical CAS and MBR systems (http://upload.wikimedia.org/wikipedia/en/thumb/c/co/MBRvsASP_Schematic.jpg/550px-MBRvsASP_Schematic.jpg)

In a CAS system, microorganisms consume organic matter in waste water inside of the aeration zone. These microorganisms then flow into a secondary clarifier where they settle out, and the water then goes on to sand filtration and disinfection while the sludge is either disposed of or recycled back into the aeration zone.

In a membrane bioreactor, microorganisms also consume organic matter in the aeration zone. However, rather than flowing on to a secondary clarifier after the aeration zone, as they would in CAS, the wastewater is filtered through a UF membrane. Judd (2008) explains that this UF membrane eliminates the need for multiple processes including secondary clarification, disinfection, and filtration, allows for higher mixed liquor suspended solids (MLSS) concentrations and therefore requires a smaller aeration zone, and requires less pumping. It can

also produce a higher quality effluent than a CAS system. For these reasons, MBRs are becoming increasingly attractive for municipal wastewater treatment, and the global market is expected to grow by 10.5% per year (Judd, 2008).

Cost Comparison: Pure PES Membrane versus SiO_2 Modified Membrane

In this analysis of an MBR system, two different designs will be discussed. The first will use the unmodified PES membrane, and the second will use the SiO_2-modified membrane. The operational costs for both these designs will be compared in a general sense. The facility will be designed to treat 1,000,000 GPD. The water treated will be the same as the water that was analyzed by Schaller, Drews, and Kraume (2010). The feed characteristics as well as several important design parameters (many of which taken from literature) are summarized in Table 7.

Table 7: Design parameters for the theoretical wastewater treatment facility. Parameters are taken from different literature sources

Category	Characteristic	Value	Source
Operational Parameters	Flow Rate (m^3/day	3785	NA
	HRT (hours)	10	NA
	F/M (kg COD/day)	0.05	Schaller et al. (2010)
	T (degrees C)	15	Marcy (2009)
	SRT (days)	40	Kraume and Drews (2010)
	Cset	2	Schaller et al. (2010)
	ρair (kg/m^3)	1.225	
Influent Conditions	S0 (mg/L)	600	
	S (mg/L)	30	
	TN (mg/L)	80	
Biokinetic Parameters	Yield (mg VSS/mg COD	0.25	Fletcher et al. (2007)
	Biological Decay Rate (b) (1/day)	0.05	

The hydraulic retention time (HRT) was chosen as 10 hours because of the effect it has on the organic loading rate (OLR). Generally, shorter HRT results in lower OLR. High OLR and low HRT can lead to increased membrane fouling and reduced treatment efficiency (Meng et al., 2007) so a reasonably high value of 10 hours was selected.

In this analysis, focus will be placed on the costs and design components that will be influenced by a membrane that is less susceptible to fouling. For example, though sludge production is an important consideration when analyzing the cost of a treatment facility, it will not be impacted by membrane fouling and therefore will not be analyzed here.

There are numerous costs associated with membrane fouling, including increased electricity demand due to increased transmembrane pressure, chemical cleaning, labor, and membrane replacement. In the case of this experiment, data do not exist to quantify how much more all these operation and maintenance requirements would cost for the pure PES membrane than they would for the SiO_2 modified membrane. Empirical, long-term tests would need to be conducted to make this assessment, as fouling is a poorly understood process and is largely dependent on feed water characteristics. For example, to determine membrane lifetime, membrane cleaning regimes, and pressure requirements, a pilot scale model would need to be built and run for, ideally, at least one year.

Nevertheless, the data that do exist demonstrate that fouling was significantly reduced in the SiO_2 membrane – it took 400 minutes to foul whereas the pure PES membrane took 20 (2000% less time), and it plateaued at a flux of approximately 2 L/m^2*h whereas the pure PES membrane plateaued around 0.4 L/m^2*h (500% lower). Therefore, it is safe to assume that costs associated with fouling would be significantly reduced in the SiO_2 modified membrane.

As a result, for this analysis, it will be assumed that five O&M costs -- electrical power, chemical cleaning, diffuser replacement, labor, and membrane replacement – will cost twice as much for the unmodified, pure PES membrane. Admittedly, this number is arbitrary and could be lower or higher. However, in terms of order of magnitude, it is accurate and will adequately quantify the degree to which reducing membrane fouling will lower costs in a MBR.

Adham, DeCarolis, and Pearce (2004) provide O&M cost estimates for various membrane processes for various flow capacities. These estimates come from a thorough survey of major MBR manufacturers, including US Filter Coproation/Jet Tech Products Group, Zenon Environmental, Inc., Ionics/Mitsubishi Rayon Corporation, and Enviroquip Inc./Kubota Corporation. These estimates for a 1 MGD plant are provided in Table 8, which also includes modified O&M costs to account for increased fouling in the pure PES membrane. For some items (such as membrane replacement and equipment repairs), cost ranges were given, so the middle of these cost ranges was used as an estimate.

Table 8: Estimated operating costs for SiO_2 and pure PES membranes (based on Adham, DeCarolis and Pearce (2004)

Item	O&M Costs $K/yr	
	Pure PES Membrane Plant	SiO2 Membrane Plant
Electrical Power for Process/Miscellaneous	140	70
Equipment Repairs/Lubricants/Replacement	36	18
Chemical Cleaning	16	8
Chemical Costs for Disinfection	4.6	4.6
Diffuser Replacement	2.4	2.4
Membrane Replacement	100	50
Labor	62	31
Total O&M Costs in First Year	368	184

As is clear from the information in Table 8, operation and maintenance costs, largely due to fouling, are significant for MBR systems; they are estimated to be $184,000 per year for a small, 1 MGD plant. Therefore, by reducing fouling, the costs of MBR systems will be significantly reduced as well.

For reference, other design parameters were calculated as well. These calculations are not highly relevant to the objectives of this experiment but are available nevertheless. They are based on the recommended design parameters in Table 7, which were taken from various sources.

Excess Sludge

To calculate how much waste sludge the system will produce, it is first important to calculate the volume of the aeration of the basin. This can be accomplished by using Equation 3 (Marcy, 2009)

$$V = Q * HRT \qquad \text{(Equation 3)}$$

where V is volume (m^3) and Q is flow rate (m^3/day).

$$V = 3{,}785 \frac{m^3}{day} * 0.417\ day$$

$$V = 1{,}580\ m^3$$

With this volume, the MLSS concentration within the aeration basin (X) can be calculated using Equation 4 (Schaller, Drews and Kraume, 2010).

$$X = \frac{1}{HRT} * \left(\frac{Y*SRT}{1+b*SRT} * (S_0 - S)\right) \quad \text{(Equation 4)}$$

$$X = \frac{1}{0.417\ day} * \left(\frac{0.25 * 40\ day}{1 + \frac{0.05}{day} * 40\ day} * \left(600\frac{mg}{L} - 30\frac{mg}{L}\right)\right)$$

$$X = 4{,}560\ \frac{mg}{L}$$

With the MLSS concentration, the amount of sludge that is wasted can be calculated using Equation 5 (Schaller, Drews and Kraume, 2010)

$$ESP = \frac{V*X}{SRT} \quad \text{(Equation 5)}$$

$$ESP = \frac{1{,}580 m^3 * 4{,}560\frac{mg}{L}}{40\ day} * \frac{L}{0.001\ m^3}$$

$$ESP = 180{,}120{,}000\ mg/day$$

$$ESP = 180\ kg/day$$

Oxygen Demand

After calculating ESP, it is possible to calculate the oxygen demand necessary to degrade the organic matter using Equation 6 (Davis and Masten, 2009). This is important as it will dictate the amount of aeration necessary for the plant, a large portion of the electricity cost.

$$M_{O2} = \frac{Q*(C_i - C_e)}{R_{COD}} - 1.42(ESP) \quad \text{(Equation 6)}$$

M_{O_2} is the mass of oxygen required by the system, R_{COD} is the ratio of COD to BOD in the wastewater, C_i is the influent COD concentration, and C_e is the effluent COD concentration. Typically, R_{COD} is approximately 2.0 (Keipper).

$$M_{O2} = \frac{3785\frac{m^3}{day} * (600 - 30)\frac{mg}{L} * \frac{L}{0.001\ m^3} * \frac{kg}{1000000\ mg}}{2} - 1.42 * (180\ kg)$$

$$M_{O2} = 823\ kg\ of\ oxygen/day$$

M_{O_2} can be converted to a volumetric flow rate ($Q_{air,\ theoretical}$) using the density of oxygen.

$$Q_{air,theoretical} = \frac{823\ kg\ O2}{1.429\ \frac{kg}{m^3}} = 576\ m^3/day$$

However, because the transfer of oxygen is not perfect, $Q_{O_2\ theoretical}$ represents only the theoretical oxygen demand. According to Fletcher, Mackley and Judd (2007), to determine how much oxygen must actually be supplied, Equations 7 and 8 must be used.

$$Q_{air\ clean\ water} = k_L a(C^* - C) \quad \text{(Equation 7)}$$

$$Q_{process} = \frac{Q_{air,clean\ water}}{\alpha\beta\varphi} \quad \text{(Equation 8)}$$

In Equation 7, k_La is the oxygen transfer coefficient, C^* is the saturated oxygen concentration (kg/m^3), and C is the dissolved oxygen concentration (kg/m^3). Schaller, Drews, and Kraume (2010) explain that k_La is dependent on the waste stream being treated and therefore should be determined empirically, so no value for k_La is shown for these calculations. Equation 8 modifies the result from Equation 7 to account for sludge properties that will disrupt the transfer of oxygen. β accounts for the effects of salts and particulates and is generally accepted to be 0.95 for conventional wastewater. ϕ accounts for the effect of temperature, and is determined using Equation 9

$$\varphi = 1.024^{(T-20)} \quad \text{(Equation 9)}$$

T is temperature in degrees C. α represents the difference between mass transfer (k_La) between clean water and process water (Fletcher, Mackley and Judd, 2007).

After calculating the air flow rate ($Q_{process}$), Jenkins provides a method to calculate the amount of horsepower that must be supplied to the blower that involves Equations 10 and 11.

$$hp = 0.01542 * \frac{Q * p_i * X}{\eta} \quad \text{(Equation 10)}$$

Where p_i is the blower inlet pressure (psia), hp is horsepower, and η is the blower efficiency (decimal form). X is the blower adiabatic factor, and is defined by Equation 11:

$$X = \left(\frac{p_d}{p_i}\right) - 1 \quad \text{(Equation 11)}$$

Where p_d is the discharge pressure (psia).

Using this method to calculate aeration requirements in addition to running empirical tests to determine how much aeration is required to reduce fouling will allow an engineer to determine the overall operating costs for an MBR system.

Capital Costs

Adham, DeCarolis and Pearce (2004) also provide a breakdown of the capital costs for an MBR system with an influent flow of 1 MGD. Table 9 shows this breakdown, and a 1 MGD plant would cost between $7,710,000 and $9,280,000.

Table 9: Breakdown of the capital costs for an MBR system

Item	Capital Cost ($K)	
	Low	High
Headworks	450	
Basins	484	
MBR System	1579	2347
Mechanical	420	
Blower and Pump building	247	
Chlorine Dosing System	217	
Subtotal	3397	4165
Electrical, 15%	510	625
Mechanical/ Plumbing/HVAC, 13%	442	541
Sitework	306	375
Subtotal	4654	5706
Contractor Overhead and Profit, 15%	698	856
Subtotal-Construction Cost	5352	6562
Land	750	
Contingency, 15%	803	984
Engineering/Legal/Administration, 15%	803	984
Total Capital Cost	**7710**	**9280**

Summary

As demonstrated by Adham, DeCarolis and Pearce (2004), fouling is a significant cost to MBR processes. By reducing fouling, operational costs reduce as well. The SiO_2 membrane prepared in this experiment fouled significantly less than the unmodified, pure PES membrane (took 20x longer to foul). However, further empirical tests need to be conducted to determine how much operational costs would decrease as a result of this enhanced antifouling performance.

Once these empirical tests are complete, the equations provided in the previous sections can be used to produce a detailed cost estimate for processes such as sludge handling and aeration. Design parameters taken from the literature and summarized in Table 7 provide all that is necessary to complete these calculations. Estimates for the capital costs of a 1 MGD plant are provided in Table 9.

References

Adham, S., DeCarolis, F., and Pearce, W. (2004). Optimization of Various MBR Systems for Water Reclamation – Phase III. *Desalination and Water Purification Research and Development Report No. 103*

Agrawal, A.Wettability, non-wettability and contact angle hysteresis. Retrieved from http://web.mit.edu/nnf/education/wettability/wetting.html

Bottino, A., Capannelli, G., & Comite, A. (2002). Preparation and characterization of novel porous PVDF-ZrO_2 composite membranes. *Desalination, 146*(1), 35-40.

Choi, J. G., Bae, T. H., Kim, J. H., Tak, T. M., & Randall, A. (2002). The behavior of membrane fouling initiation on the crossflow membrane bioreactor system. *Journal of Membrane Science, 203*(1), 103-113.

Cuperus, F., & Smolders, C. (1991). Characterization of UF membranes: Membrane characteristics and characterization techniques. *Advances in Colloid and Interface Science, 34*(2), 135-173. DaRo UV Systems LTD.UV water treatment. Retrieved from http://www.uvwatertreatment.co.uk/images/DNA.jpg

Davis, M. L., & Masten, S. J. (2004). *Principles of environmental engineering and science* McGraw-Hill New York, NY.

DLVO theory image. Retrieved from http://www.malvern.com/labeng/industry/colloids/dlvo_theory_1.jpg

Genne, I., Kuypers, S., & Leysen, R. (1996). Effect of the addition of ZrO_2 to polysulfone based UF membranes. *Journal of Membrane Science, 113*(2), 343-350.

Goosen, M., Sablani, S., Al-Hinai, H., Al-Obeidani, S., Al-Belushi, R., & Jackson, D. (2005). Fouling of reverse osmosis and ultrafiltration membranes: A critical review. *Separation Science and Technology, 39*(10), 2261-2297.

Fletcher, H., Mackley, T., & Judd, S. (2007). The cost of a package plant membrane bioreactor. *Water Research, 41*(12), 2627-2635.

Huang, J., Zhang, K., Wang, K., Xie, Z., Ladewig, B., & Wang, H. (2012). Fabrication of polyethersulfone-mesoporous silica nanocomposite ultrafiltration membranes with antifouling properties. *Journal of Membrane Science*

Jenkins, T. *Evaluating and comparing aeration blower power requirements.* Wastewater Solutions, Dresser Roots.

Jing-Feng Li, J. F., Xu, Z. L., Yang, H., Yu, L. Y., & Liu, M. (2009). Effect of TiO_2 nanoparticles on the surface morphology and performance of microporous PES membrane. *Applied Surface Science, 255*(9), 4725-4732.

Judd, S. (2008). The status of membrane bioreactor technology. *Trends in Biotechnology, 26*(2), 109-116.

Kiepper, B. Understanding laboratory wastewater tests: I. organics (BOD, COD, TOC, O&G). *CAES Publications* Kools, W. F. C. (1998). *Membrane formation by phase inversion in multicomponent polymer systems. mechanisms and morphologies* Universiteit Twente.

Li, J. H., Xu, Y. Y., Zhu, L. P., Wang, J. H., & Du, C. H. (2009). Fabrication and characterization of a novel TiO_2 nanoparticle self-assembly membrane with improved fouling resistance. *Journal of Membrane Science, 326*(2), 659-666.

Marcy, C. (2009). *The Effects of Hydrophobic and Hydrophilic Natural Organic Matter on Charged Ultrafiltration Performance*. WPI Major Qualifying Project.

Marshall, A., Munro, P., & Trägårdh, G. (1993). The effect of protein fouling in microfiltration and ultrafiltration on permeate flux, protein retention and selectivity: A literature review. *Desalination, 91*(1), 65-108.

Matar, O., Hewitt, G., & Ortiz, E.Phase inversion in liquid-liquid dispersions. *Department of Chemical Engineering, Imperial College, London*

Matsuura, T. (1994). *Synthetic membranes and membrane separation processes* CRC PressI Llc.

McCabe, W. L., Smith, J. C., & Harriott, P. (1956). *Unit operations of chemical engineering* McGraw-Hill Book Company New York.

Maximous, N., Nakhla, G., Wan, W., & Wong, K. (2010). Performance of a novel ZrO_2/PES membrane for wastewater filtration. *Journal of Membrane Science, 352*(1), 222-230.

Mcintyre, N. (2012,). How ill climate change impact on fresh water scarcity. *The Guardian*

Membrane structure: SEM images. Retrieved from http://ars.els-cdn.com/content/image/1-s2.0-S1570023204001345-gr1.jpg

Meng, F., Chae, S. R., Drews, A., Kraume, M., Shin, H. S., & Yang, F. (2009). Recent advances in membrane bioreactors (MBRs): Membrane fouling and membrane material. *Water Research, 43*(6), 1489-1512.

National Geographic (2013). Freshwater Crisis. National Geographic Website.

Pereira, L. S., Cordery, I., & Iacovides, I. (2009). *Coping with water scarcity: Addressing the Challenges.* Springer.

Population Institute (2010). Population and Water.

Poyatos, J., Muñio, M., Almecija, M., Torres, J., Hontoria, E., & Osorio, F. (2010). Advanced oxidation processes for wastewater treatment: State of the art. *Water, Air, and Soil Pollution, 205*(1-4), 187-204.

Queen Mary University of London.5.3 photoelectron spectroscopy. Retrieved from http://www.chem.qmul.ac.uk/surfaces/scc/scat5_3.htm

Reihanian, H., Robertson, C., & Michaels, A. (1983). Mechanisms of polarization and fouling of ultrafiltration membranes by proteins. *Journal of Membrane Science, 16*, 237-258.

Saddat, A. (2011). *Preparation, characterization and performance optimization of ultrafiltration membranes produced with polymeric and inorganic additives.* ().Worcester Polytechnic Institute.

Schaller, J., Drews, A., & Kraume, M. (2010). Development of a cost model for membrane bioreactors including sludge handling costs. *Desalination and Water Treatment, 18*(1-3), 315-320.

Sewerage Business Management Centre.Advanced oxidation process with hydrogen peroxide. Retrieved from http://www.sbmc.or.jp/english/ozonation_technology.files/image002.jpg

Shen, J., Ruan, H., Wu, L., & Gao, C. (2011). Preparation and characterization of PES–SiO_2 organic–inorganic composite ultrafiltration membrane for raw water pretreatment. *Chemical Engineering Journal, 168*(3), 1272-1278.

Shen, L., Bian, X., Lu, X., Shi, L., Liu, Z., Chen, L., . . . Fan, K. (2012). Preparation and characterization of ZnO/polyethersulfone (PES) hybrid membranes. *Desalination, 293*, 21-29

Su, Y., Huang, C., Pan, J., Hsieh, W., & Chu, M. (2011). Fouling mitigation by TiO2 composite membrane in membrane bioreactors. *Journal of Environmental Engineering, 138*(3), 344-350.

Turral, H., Burke, J. J., & Faurès, J. (2011). *Climate change, water and food security.* Food and Agriculture Organization of the United Nations.

United States Environmental Protecation Agency. (1999). Wastewater Technology fact sheet: Ultraviolet disinfection

United States Environmental Protection Agency. (1999). EPA guidance manual: Chapter 8 ultraviolet radiation., 8-1.

Wikipedia. (2010). Contact angle image file. Retrieved from http://en.wikipedia.org/wiki/File:Contact_angle.svg

Word Health Organization. (2009). 10 facts about water scarcity.

World Water Organization (2010). Water Facts & Water Stories from Across the Globe.

Wu, G., Gan, S., Cui, L., & Xu, Y. (2008). Preparation and characterization of PES/TiO_2 composite membranes. *Applied Surface Science, 254*(21), 7080-7086.

Xu, Z., Yu, L., & Han, L. (2009). Polymer-nanoinorganic particles composite membranes: A brief overview. *Frontiers of Chemical Engineering in China, 3*(3), 318-329.

Yu, H. Y., Hu, M. X., Xu, Z. K., Wang, J. L., & Wang, S. Y. (2005). Surface modification of polypropylene microporous membranes to improve their antifouling property in MBR: NH_3 plasma treatment. *Separation and Purification Technology, 45*(1), 8-15.

Zhou, H., & Smith, D. W. (2002). Advanced technologies in water and wastewater treatment. *Journal of Environmental Engineering and Science, 1*(4), 247-264.

Appendix 1: Information on Methodology

Table 10: Mass of components in the pure PES casting solution

Component	Mass (g)
PES	89.1
DMAc	376
PEG 400	29.7

Table 11: Mass of components in the pure PES-TiO_2 casting solution

Component	Mass (g)
PES	90.24
DMAc	376
PEG 400	30.1
TiO_2	5.01

Table 12: Mass of components in the pure PES-SiO_2 casting solution

Component	Mass (g)
PES	90.24
DMAc	376
PEG 400	30.1
SiO_2	5.01

Table 13: Mass of components in the pure PES-ZnO casting solution

Component	Mass (g)
PES	90.24
DMAc	376
PEG 400	30.1
ZnO	5.01

Table 14: Mass of components in the pure PES-ZrO_2 casting solution

Component	Mass (g)
PES	90.24
DMAc	376
PEG 400	30.1
ZrO_2	5.01

Appendix 2: Raw Data

Contact Angle Data

Table 15: Contact angle data

	Contact Angle	Standard Deviation	% Reduction Contact Angle
PES	67.69	5.44	0
PES+SiO2	62.36	3.92	7.874132073
PES+TiO2	62.05	3.81	8.332102231
PES+ZnO	58.56	4.75	13.48795982
PES+ZrO2	62.53	3.28	7.622987147

Pure Water Flux Data

Table 16: Pure water flux of all five membranes before BSA filtration

	Time to filter 40g pure H2O no BSA (s)	Mass Flow Rate (g/min)	Mass Flow Rate (g/hr)	Volumetric Flow Rate (L/hr)	Flux (L*m^-2*hr^-1)
Pure PES	261.02	9.194697724	551.6818635	0.551681863	161.3104864
SiO2	94.17	25.48582351	1529.149411	1.529149411	447.1197107
TiO2	117.33	20.45512657	1227.307594	1.227307594	358.8618696
ZnO	124.22	19.3205603	1159.233618	1.159233618	338.9571982
ZrO2	103.83	23.11470673	1386.882404	1.386882404	405.5211707

Table 17: Pure water flux of pure water directly after BSA filtration

	Time to filter 40g pure H2O post BSA filtration (s)	Mass Flow Rate (g/min)	Mass Flow Rate (g/hr)	Volumetric Flow Rate (L/hr)	Flux (L*m^-2*hr^-1)
Pure PES	2163.49	1.10931874	66.55912438	0.066559124	19.46173227
SiO2	882.81	2.718591769	163.1155062	0.163115506	47.69459245
TiO2	753.02	3.187166344	191.2299806	0.191229981	55.91519901
ZnO	676.95	3.545313539	212.7188123	0.212718812	62.19848313
ZrO2	614.18	3.907649223	234.4589534	0.234458953	68.55524953

Table 18: Pure water flux of all five membranes after BSA filtration and after membrane cleaning with pure water

	Time to filter 40g pure H2O post pure H2O cleaning (s)	Mass Flow Rate (g/min)	Mass Flow Rate (g/hr)	Volumetric Flow Rate (L/hr)	Flux (L*m^-2*hr^-1)
Pure PES	1590.04	1.50939599	90.5637594	0.090563759	26.4806314
SiO2	387.64	6.191311526	371.4786916	0.371478692	108.6195005
TiO2	490.2	4.895960832	293.7576499	0.29375765	85.89404969
ZnO	461.92	5.195704884	311.742293	0.311742293	91.15271726
ZrO2	484.8	4.95049505	297.029703	0.297029703	86.85079034

Flux Recovery Data

Table 19: Flux recovery data

	Initial flux pure H2O	Pure H2O flux post BSA	Pure H2O flux post cleaning and post BSA	Flux Recovery Ratio	Irreversible Flux Loss	Initial Flux Reduction
Pure PES	161.3104864	19.46173227	26.4806314	16.41593922	83.58406078	87.93523427
SiO2	447.1197107	47.69459245	108.6195005	24.2931586	75.7068414	89.33292554
TiO2	358.8618696	55.91519901	85.89404969	23.93512852	76.06487148	84.41874054
ZnO	338.9571982	62.19848313	91.15271726	26.89210253	73.10789747	81.65004801
ZrO2	405.5211707	68.55524953	86.85079034	21.41707921	78.58292079	83.09453255

Porosity

Table 20: Volume data for the exterior of all five membranes

	Thickness (0.01 mm)	Thickness (mm)	Thickness (m)	Volume Membrane (m^3)
PES 1	11	0.11	0.00011	5.22805E-08
PES 2	11	0.11	0.00011	5.22805E-08
PES 3	11	0.11	0.00011	5.22805E-08
SiO2 1	16	0.16	0.00016	7.60444E-08
SiO2 2	17	0.17	0.00017	8.07972E-08
SiO2 3	17	0.17	0.00017	8.07972E-08
ZrO2 1	19	0.19	0.00019	9.03027E-08
ZrO2 2	17	0.17	0.00017	8.07972E-08
ZrO2 3	17	0.17	0.00017	8.07972E-08
ZnO 1	18	0.18	0.00018	8.555E-08
ZnO 2	16	0.16	0.00016	7.60444E-08
ZnO 3	17	0.17	0.00017	8.07972E-08
TiO2 1	18	0.18	0.00018	8.555E-08
TiO2 2	18	0.18	0.00018	8.555E-08
TiO2 3	18	0.18	0.00018	8.555E-08

Table 21: Volume data for the water within all five membranes

	Wet Weight (g)	Dry Weight (g)	Mass Water (g)	Volume Water (m^3)
PES 1	0.063	0.0154	0.0476	4.76E-08
PES 2	0.0545	0.0153	0.0392	3.92E-08
PES 3	0.0497	0.014	0.0357	3.57E-08
SiO2 1	0.0643	0.0152	0.0491	4.91E-08
SiO2 2	0.0596	0.0165	0.0431	4.31E-08
SiO2 3	0.0586	0.0159	0.0427	4.27E-08
ZrO2 1	0.092	0.0175	0.0745	7.45E-08
ZrO2 2	0.0747	0.0156	0.0591	5.91E-08
ZrO2 3	0.0675	0.0154	0.0521	5.21E-08
ZnO 1	0.076	0.0164	0.0596	5.96E-08
ZnO 2	0.0696	0.016	0.0536	5.36E-08
ZnO 3	0.0794	0.0164	0.063	0.000000063
TiO2 1	0.0793	0.0171	0.0622	6.22E-08
TiO2 2	0.0786	0.0182	0.0604	6.04E-08
TiO2 3	0.0676	0.0156	0.052	0.000000052

Table 22: Summary of membrane porosity

Volume Water (m^3)	Volume Membrane (m^3)	Porosity	Average Porosity
4.76E-08	5.22805E-08	0.910	0.781
3.92E-08	5.22805E-08	0.750	
3.57E-08	5.22805E-08	0.683	
4.91E-08	7.60444E-08	0.646	0.569
4.31E-08	8.07972E-08	0.533	
4.27E-08	8.07972E-08	0.528	
7.45E-08	9.03027E-08	0.825	0.734
5.91E-08	8.07972E-08	0.731	
5.21E-08	8.07972E-08	0.645	
5.96E-08	8.555E-08	0.697	0.727
5.36E-08	7.60444E-08	0.705	
0.000000063	8.07972E-08	0.780	
6.22E-08	8.555E-08	0.727	0.680
6.04E-08	8.555E-08	0.706	
0.000000052	8.555E-08	0.608	

Viscosity

Table 23: Viscosity data for the pure PES casting solution

PES		
RPM	**cP**	**%**
10	477	15.8
12	483	19.3
20	488	32.6
30	500	50
50	507	84.5

Table 24: Viscosity data for the pure SiO_2 casting solution

SiO2		
RPM	**cP**	**%**
10	447	14.9
12	450	18
20	459	30.6
30	470	47
50	474	79

Table 25: Viscosity data for the TiO_2 casting solution

TiO2		
RPM	cP	%
6	560	11.2
10	594	19.8
12	600	24
20	606	40.4
30	618	61.8

Table 26: Viscosity data for the ZnO casting solution

ZnO		
RPM	**cP**	**%**
12	527	21.1
20	543	36.2
30	553	55.3

Table 27: Viscosity data for the ZrO_2 casting solution

ZrO2		
RPM	**cP**	**%**
10	456	15.2
12	463	18.5
20	473	31.5
30	482	48.2
50	487.2	40.4

Mechanical Properties

Breaking Force

Table 28: Breaking force raw data

	BREAKING FORCE (MPa)					AVERAGE	STDEV
PES	5.8423	6.55688	6.22018	6.27835	6.43263	6.266068	0.27117817
PES+SiO2	2.24217	2.45594	1.98811	2.73231	2.14001	2.311708	0.29014665
PES+TiO2	2.48699	2.69052	1.89974	2.87564	3.11571	2.61372	0.46160649
PES+ZnO	2.04653	2.05077	2.5034	2.01726	2.24855	2.173302	0.20619244
PES+ZrO2	2.09308	2.24038	2.77149	2.19592	2.3208	2.324334	0.26314341

Elongation Rate

Table 29: Elongation rate raw data

	ELONGATION RATE (%)					AVERAGE	STDEV
PES	11.6305	15.3347	12.5917	21.8507	20.0742	16.29636	4.51503912
PES+SiO2	6.25809	10.1861	8.92578	10.9996	7.44431	8.762776	1.94085082
PES+TiO2	6.22101	6.51836	4.29658	10.0363	17.2956	8.87357	5.1433077
PES+ZnO	9.51747	5.62978	8.2972	8.18476	8.26013	7.977868	1.42375741
PES+ZrO2	8.85111	7.07436	8.77764	9.11111	9.62845	8.688534	0.96202145

Appendix 3: Calibration Curves

Table 30: Data for BSA calibration curve

Concentration (mg/L)	Absorbance
0	0
10	0.014
100	0.071
200	0.129
400	0.244
700	0.442
1000	0.637

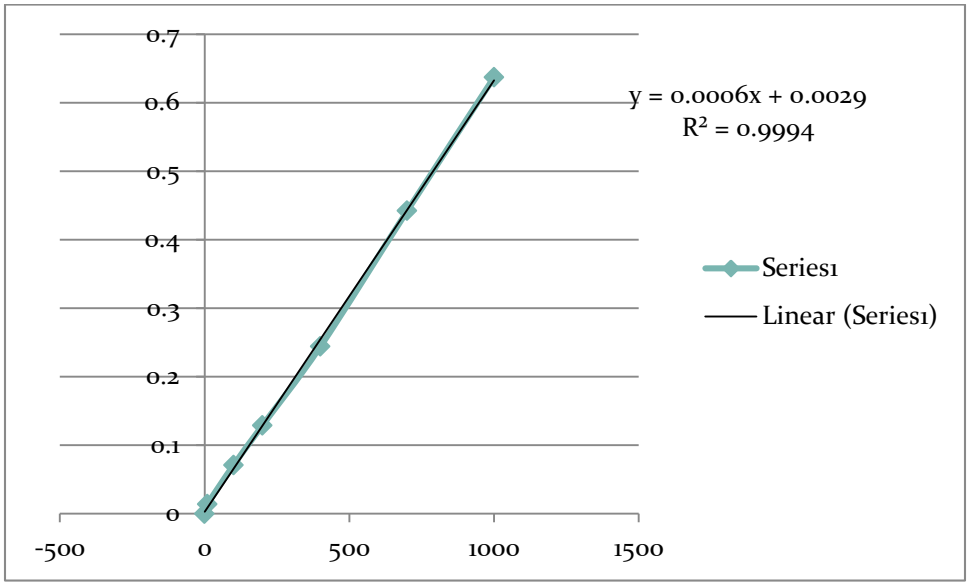

Figure 43: BSA calibration curve, which was generated using the data in Table _